ADVANCES IN ATMOSPHERIC SCIENCES, VOL. 39, JANUARY 2022, 22–54

• **Review** •

Impacts of Oceanic Fronts and Eddies in the Kuroshio-Oyashio Extension Region on the Atmospheric General Circulation and Storm Track

Guidi ZHOU[*1,2] and Xuhua CHENG[1,2,3]

[1]*Key Laboratory of Marine Hazards Forecasting*, *Ministry of Natural Resources (MNR)*, *Hohai University*, *Nanjing* 210098, *China*

[2]*College of Oceanography*, *Hohai University*, *Nanjing* 210098, *China*

[3]*Southern Marine Science and Engineering Guangdong Laboratory (Zhuhai)*, *Zhuhai* 519080, *China*

(Received 28 November 2020; revised 14 July 2021; accepted 2 August 2021)

ABSTRACT

This paper reviews the progress in our understanding of the atmospheric response to midlatitude oceanic fronts and eddies, emphasizing the Kuroshio-Oyashio Extension (KOE) region. Oceanic perturbations of interest consist of sharp oceanic fronts, temperature anomalies associated with mesoscale eddies, and to some extent even higher-frequency submesoscale variability. The focus is on the free atmosphere above the boundary layer. As the midlatitude atmosphere is dominated by vigorous transient eddy activity in the storm track, the response of both the time-mean flow and the storm track is assessed. The storm track response arguably overwhelms the mean-flow response and makes the latter hard to detect from observations. Oceanic frontal impacts on the mesoscale structures of individual synoptic storms are discussed, followed by the role of oceanic fronts in maintaining the storm track as a whole. KOE fronts exhibit significant decadal variability and can therefore presumably modulate the storm track. Relevant studies are summarized and intercompared. Current understanding has advanced greatly but is still subject to large uncertainties arising from inadequate data resolution and other factors. Recent modeling studies highlighted the importance of mesoscale eddies and probably even submesoscale processes in maintaining the storm track but confirmation and validation are still needed. Moreover, the atmospheric response can potentially provide a feedback mechanism for the North Pacific climate. By reviewing the above aspects, we envision that future research shall focus more upon the interaction between smaller-scale oceanic processes (fronts, eddies, submesoscale features) and atmospheric processes (fronts, extratropical cyclones etc.), in an integrated way, within the context of different climate background states.

Key words: atmospheric response, storm track, oceanic front, mesoscale eddy, submesoscale, Kuroshio-Oyashio Extension

Citation: Zhou, G. D., and X. H. Cheng, 2022: Impacts of oceanic fronts and eddies in the Kuroshio-Oyashio Extension region on the atmospheric general circulation and storm track. *Adv. Atmos. Sci.*, **39**(1), 22–54, https://doi.org/10.1007/s00376-021-0408-4.

Article Highlights:

- The progress and remaining issues on the atmospheric impacts of oceanic fronts and mesoscale eddies are reviewed.
- Oceanic fronts modify atmospheric transient eddies and influence its circulation, yet there still lacks a consensus.
- Mesoscale eddies and smaller-scale ocean perturbations could possibly exert a rectified influence on the atmospheric storm track.

1. Introduction

The Kuroshio-Oyashio Extension (KOE, 32°–45°N, 140°–180°E) region is the confluence region between the warm Kuroshio Extension (KE) and the cold Oyashio Extension (OE), the two major western boundary currents in the North Pacific Ocean. This region lies beneath the atmospheric westerly jet and the entrance of the midlatitude storm track comprising vigorous baroclinic transient eddy (storm) activity (Chang and Orlanski, 1993; Chang et al., 2002). Oceanic processes in this region are characterized by the powerful KE and OE currents, several oceanic fronts (Yasuda, 2003; Kida et al., 2015), and an abundance of meso-

* Corresponding author: Guidi ZHOU
Email: guidi.zhou@hhu.edu.cn

scale eddies (Williams et al., 2007) driven by complex oceanic dynamics. These mesoscale processes are associated with thermodynamic variability in terms of sea surface temperature (SST), upper ocean heat content, and air-sea heat flux (e.g., Chelton et al., 2004; Minobe et al., 2008; Frenger et al., 2013; Chen et al., 2017; Sugimoto et al., 2017). Because of the rich oceanic and atmospheric multiscale processes, air-sea interaction in this region is of great interest to the oceanography and meteorology communities.

The problem of midlatitude atmosphere-ocean interaction in the vicinity of the western boundary currents and their eastward extensions involves four main factors: oceanic circulation (currents and jets), mesoscale ocean perturbations (fronts and eddies), atmospheric circulation (pressure and wind), and atmospheric transient eddies (storm track). Each of these is complex and dynamic. The atmospheric storm track and circulation, as well as their interaction, have been extensively studied in meteorology for decades (briefly introduced in section 3), yet our current knowledge on mesoscale ocean perturbations and their interaction with the oceanic jets is still limited (see section 2). The characteristics and mechanisms for the two-way atmosphere-ocean interaction, namely the oceanic response to wind anomalies and the atmospheric response to changes of oceanic jets and mesoscale perturbations, are each under active research. This paper serves as a review for the upward branch of air-sea interaction in the KOE, i.e., the atmospheric response to oceanic perturbations. Here, we are more interested in the response of the whole troposphere, not just the surface boundary layer. Of the components of oceanic perturbations, we focus on the mesoscale, i.e., the fronts and eddies, although oceanic jets must also be included because of their tight dynamical connection with the mesoscale. It has been found that by means of anomalous heat flux forcing, mesoscale oceanic perturbations are able to exert significant modulation on the overlying atmosphere, both in terms of atmospheric mean flow (Minobe et al., 2008, 2010; Bryan et al., 2010; Kuwano-Yoshida et al., 2010; Shimada and Minobe, 2011) and transient eddies (Nakamura et al., 2008; Booth et al., 2012; Sheldon et al., 2017; Vannière et al., 2017a; Small et al., 2019). The transient eddy response then drives further changes to the mean-flow by the forcing of eddy fluxes (Hoskins, 1983; Peng et al., 1997; Peng and Whitaker, 1999; Kushnir et al., 2002). The problem of atmospheric response to mesoscale oceanic perturbations is particularly difficult because of the multiscale oceanic and atmospheric processes involved. This requires that the resolution of observational data and numerical models be sufficiently high to represent the mesoscale processes of the ocean and their atmospheric impacts, which has only become possible in recent years.

Fortunately, a similar problem—atmospheric response to midlatitude large-scale ocean perturbations has been studied extensively since the 1980s. This latter problem involves the same atmospheric processes as those currently discussed, with only the scale of the ocean forcing being different. Therefore, a lot can be learned from the findings of the large-scale problem. It is, in fact, through the advance of the large-scale problem that the importance of the mesoscale problem was initially appreciated. For comprehensive reviews on the atmospheric response to midlatitude large-scale ocean perturbations, please refer to the now-classic work of Kushnir et al. (2002), and the recent update of Zhou (2019). Basically, it is now well established that the atmospheric response to midlatitude large-scale oceanic perturbations (primarily SST anomalies) is mediated by the transient baroclinic eddies. SST anomalies force changes in the storm track strength and location, and storm track changes further drive a general circulation response. The problem thus largely boils down to the storm track response to SST anomalies. Among the various aspects of midlatitude SST anomalies, it has been found that SST fronts have the ability to maintain the storm track by sustaining low-level baroclinicity, therefore perturbations to SST fronts drive storm track responses (Nakamura et al., 2004, 2008; Sampe et al., 2010; see section 5.2). The influence of midlatitude SST fronts on the storm track has received increased research attention and was later extended to the influence of mesoscale eddies, which can be envisioned as circular fronts.

The current research on atmospheric response to midlatitude oceanic fronts and eddies can be divided into four groups, all of which are reviewed in this paper.

First, there is a large body of research on the response of atmospheric basic flow to oceanic fronts and eddies. Such response is thermally direct, not mediated by the storm track. This eddy-free response is traditionally believed to be confined to the marine atmospheric boundary layer (MABL). Please see Small et al. (2008) for a thorough review of the MABL response. Starting from the beginning of this century, several studies showed evidence of a free-atmospheric response to midlatitude mesoscale SST features too. Section 4.1 reviews this issue. However, more recently, scientists started arguing that the free-atmospheric basic-flow response is just a rectified effect of the transient eddy response. The progress and debate are reviewed in section 4.2.

Second, the influence of oceanic fronts on individual atmospheric eddies (extratropical cyclones and anticyclones) and their statistics (the storm track) has received much research interest. The exact mechanism of oceanic frontal impacts on cyclones, particularly on different parts of the cyclone structure, is still poorly known. Current research on this issue is still scarce and premature (section 5.1). Storm track response to oceanic fronts, on the other hand, has been more extensively studied, primarily through idealized model experiments. Although the importance of oceanic fronts has been acknowledged, the mechanism is still under debate. Sections 5.2–5.4 review the current progress on this issue.

Third, it has been found that the decadal variation of KOE fronts can drive decadal modulation on the storm track and atmospheric circulation. Current studies are mainly

based on reanalysis data and numerical experiments, focusing on the impacts of the OE front, as it has a much stronger and larger-scale SST gradient than the KE front. However, large controversy exists in the findings, arguably due to the inadequate data resolution and questionable statistical methods, as well as the different time periods being investigated. Also, studies on the impacts of the decadal KE variation are rare and subject to large uncertainties. Overall, so far, the importance of the KE and OE fronts in modulating the storm track on decadal timescales is basically a given, yet a consensus on the characteristics and mechanism is still lacking. Please see section 6 for details.

Last, in recent years a few modeling studies proposed that aside from oceanic fronts, the accumulative effects of KOE mesoscale eddies might be important in maintaining the storm track as well, therefore having the potential to exert significant large-scale and remote atmospheric impacts. Such studies are still very scarce, and they lack observational support. Section 7 reviews the current understanding and discusses the possible implications.

Based on the state-of-the-art, albeit incomplete, understanding of the oceanic mesoscale processes themselves and their atmospheric impacts, some studies have already found evidence that the modulation of KOE fronts on the storm track could be an integral part of the North Pacific decadal climate variability. Coupled empirical climate prediction models are developed by that means, although the current prediction skill is still relatively low. The progress on such models is reviewed in section 8.

Given the numerous research efforts which sometimes yield conflicting and perplexing results, we believe it is timely to review the currently available studies, make an informative comparison of their results, organize the knowns and the unknowns, and try to provide insights for future research. This paper is an attempt to that end. Here, general aspects of frontal and mesoscale eddy impacts on the atmosphere are reviewed based on studies regarding both the Gulf Stream frontal zone in the North Atlantic and the KOE fronts and eddies in the North Pacific, and to a lesser degree the Agulhas frontal zone in the Southern Indian Ocean. However, we will focus primarily on the KOE, especially when discussing the decadal atmospheric modulation of oceanic fronts and eddies, since the KOE has a better-established decadal cycle than the Gulf Stream, thanks to the broader basin of the North Pacific (Kwon et al., 2010; Kelly et al., 2010). It should be noted again that in this paper, we restrict ourselves to the large-scale, free-atmospheric, and storm track impacts of oceanic mesoscale features, with the MABL influences only briefly introduced when it is of direct relevance to the free-atmosphere and storm track. This paper will pay more attention to boreal winter when air-sea interaction over the midlatitude oceans is the strongest (Davis, 1976, 1978; Wallace and Jiang, 1987; Kushnir et al., 2002), and seasonal differences will be briefly discussed when necessary as a complement.

The remainder of this paper is organized as follows. Section 2 briefly introduces the currents, fronts, eddies in the KOE region, and the possible mechanisms of the decadal KE variability. Section 3 introduces some basic knowledge for storm track dynamics and the knowledge obtained historically from the problem of atmospheric response to large-scale SST anomalies. Section 4 reviews the oceanic frontal imprints upon the free-atmospheric mean flow, and the recent debate over its very existence. Section 5 focuses on the role of ocean fronts to both the individual storms and their statistics—the storm track, as usually revealed by idealized model experiments. Next, the decadal modulation of the KOE fronts on the atmosphere is discussed in section 6 from observational and modeling perspectives, with a discussion on seasonal contrast and background state sensitivity. Section 7 introduces recent findings on, and future implications of, mesoscale eddy impacts on the storm track. Section 8 briefly introduces the North Pacific decadal climate feedback theory bridged by the storm track response to KOE fronts. Finally, section 9 summarizes the current findings and provides a discussion on the gaps and outlook. We note here that although we try to cite as many relevant papers as we could, this paper is by no means comprehensive.

2. Currents, fronts, and eddies in the KOE region

The KOE region consists of the Kuroshio Extension (KE), the Oyashio Extension (OE), and the Kuroshio-Oyashio Confluence (KOC) region in between. It is a complex multi-scale system, yet the current knowledge on the dynamics and thermodynamics of the system is still poor (Qiu, 2001; Yasuda, 2003; Kida et al., 2015). Here, we briefly introduce only the most important recent understandings to the KOE system that are relevant to the issue of its atmospheric impacts. More detailed information about the characteristics and physical mechanisms of the KOE variability should be found in other studies, e.g., the reviews by Kwon et al. (2010), Kelly et al. (2010), and Kida et al. (2015).

2.1. *The KE, OE, and their associated fronts*

The KE is a strong baroclinic inertial current, with pronounced sea level anomalies and thus can be easily identified from the sea surface height (SSH) field (Fig. 1a). In fact, the KE axis is often approximated using a certain SSH contour (e.g., Qiu and Chen, 2006). The KE is associated with vigorous mesoscale eddy activity (Fig. 1b), as well as a sharp SST gradient, namely the KE front (KEF, Fig. 1c). The KEF peaks at subsurface levels below the mixed layer (e.g., Kida et al., 2015). In terms of SST gradient, the KEF always appears slightly to the north of the KE, its axis generally following the axis of KE, but the two are not exactly the same (Chen, 2008). Decadal fluctuations of the KE and KEF are basically simultaneous (Fig. 2a), both much stronger than their respective seasonal variability (Chen,

2008; Seo et al., 2014; Wang et al., 2016).

The OE, in contrast, does not have noticeable sea level signatures (Fig. 1a), owing to the coexistence of a strong temperature front (the OEF) and a salinity front, whose contributions to density largely cancel out (Yuan and Talley, 1996). The OEF is shallower than the KEF, but its SST gradient is stronger and spans a longer distance, with two branches east and west of 153°E known as the OEF-W and OEF-E (Fig. 1c, Nonaka et al., 2006; Kida et al., 2015). The area where the OEF is located is sometimes referred to as the subarctic frontal zone (SAFZ, roughly 37.5°–42.5°N, 147.5°–160.5°E). Usually, it is believed that the OEF migrates meridionally by 1°–2° on decadal timescales (Belkin et al., 2002; Nakamura and Kazmin, 2003; Nonaka et al., 2006, 2008; Taguchi et al., 2012; Wagawa et al., 2014). Its latitudinal position, defined by the latitude of the maximum SST gradient, is positively correlated to the average SST in the SAFZ (Taguchi et al., 2012). However, there are also arguments that the OEF does not move (Nakano et al., 2018), or that the northward shift is, in fact, a northward broadening of the frontal zone, with its strength (the maximum gradient) remaining the same (Smirnov et al., 2015).

The KEF and OEF both exhibit significant interannual-to-decadal variability (Fig. 1d).

2.2. *The KE bimodal dynamical system*

Since satellite altimeter data became available, many research endeavors have confirmed that the KE exhibits bimodal variability on decadal timescales, i.e., it switches between a stable mode and an unstable mode (Qiu and Chen, 2005, 2010; Qiu et al., 2007; Taguchi et al., 2007; Ceballos et al., 2009; Sugimoto and Hanawa, 2009; Kelly et al., 2010; Sugimoto et al., 2014). Here, we introduce the KE bimodal variability based on the framework of Qiu et al. (2017) who also considered the OEF branches. It is argued that the KE stable mode begins when SSH anomalies generated by the basin-scale wind stress curl propagate to the western boundary and enhance the KE's southern recirculation gyre, making the KE current stronger and displacing its position northward. This enhances warm water transport into the east part of the KOC and the SAFZ, thus increasing the SAFZ SST (Isoguchi et al., 2006; Sugimoto et al., 2014;

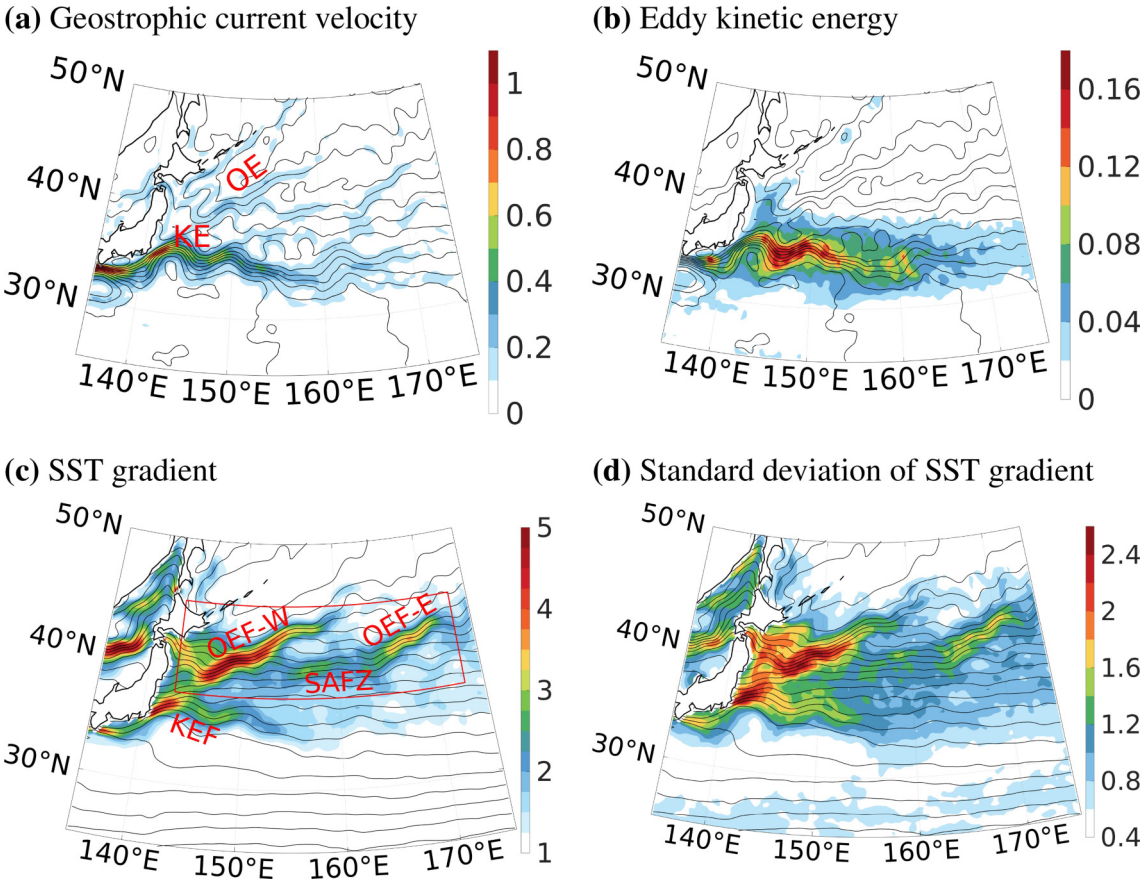

Fig. 1. The 1993–2016 mean (a) geostrophic current velocity (m s^{-1}, shading) and SSH (contours; CI = 0.1 m); (b) eddy kinetic energy (m^2 s^{-2}, shading) and SSH (contours; CI = 0.1 m) based on the AVISO daily satellite altimeter data. Eddy kinetic energy is defined as $\left(u'^2+v'^2\right)/2$, where the prime denotes the 300-day high-pass filtered data. Shown in (a) are also the position of the KE and OE. The 1981–2016 mean (c) SST gradient [°C (100 km)$^{-1}$, shading] and SST (contours; CI = 1°C); (d) interannual standard deviation of SST (°C, shading) and SST (contours; CI = 1°C) based on the NOAA daily OISST blended satellite and in-situ data. Shown in (c) are also the position of the KEF and branches of the OEF and the approximate area of the SAFZ.

Wagawa et al., 2014). On the other hand, the basin-scale wind stress variability also drives the mid-basin SSH anomaly in subarctic latitudes, which propagates westward at approximately half the speed of its midlatitude counterpart. At the time when the SAFZ SST is increased, the subarctic anomaly arrives at the western boundary and accelerates the subarctic current, transporting more cold water to the north of the OEF-E. Together with the concurrent warm water transport enhancement to the south, the OEF-E is strengthened. In the meantime, the more northerly latitude of the KE jet during the stable mode allows the deep-reaching KE to flow over a deep passage in the northern part of the Shatsky Rise, a seamount located at 158°–160°E. Due to the weaker jet-topography interaction, the KE axis is straighter and mesoscale eddy activity in the western KOC is reduced. With a delay of 2.5 years (a quarter of the decadal cycle), the reduced mesoscale perturbations decrease the western KOC SST as a result of the lessened poleward heat transport by eddies (Sugimoto and Hanawa, 2011; Seo et al., 2014; Sugimoto et al., 2014; Masunaga et al., 2016), and the OEF-W is therefore weakened. The unstable mode of KE, on the other hand, is associated with a southerly position over the shallower part of the Shatsky Rise, resulting in a more convolved path and an increased presence of topographically-generated mesoscale eddies. The corresponding OEF-E is weaker, but OEF-W is stronger. However, it should be noted that while the arguments about KE strength, position, path length, and eddy variability and correlation are basically solid (Fig. 2b), the association between the KE and the OEF branches is not yet thoroughly tested. Qiu et al. (2017) used the time series of the leading principal component to create indices of OEF-W/E position, which explains only 22% and 14.7% of the respective total variance. The small explained variance reflects the complexity of the OEF variability and its association with the KE. More in-depth investigation into the KOE dynamical system is clearly needed but is beyond the scope of this review paper on oceanic impacts on the atmosphere.

2.3. *Mechanism for KE decadal variability*

The above discussions on decadal variability of the KOE system rely on the idea that decadal KE variability is essentially forced by the arrival of zonally-propagating sea level anomalies driven by basin-scale wind stress anomalies at the same latitude, which is indeed a well-received argument (Miller et al., 1998; Deser et al., 1999; Xie et al., 2000; Seager et al., 2001; Qiu, 2002, 2003; Qiu and Chen, 2005; Taguchi et al., 2005). However, other mechanisms emphasizing the role of oceanic intrinsic variability do exist. Since this review paper focuses on the atmospheric response to decadal KE variability, not the generating mechanism of the KE variability per se, here, we only briefly introduce the mechanisms of KE variability that have been proposed in the literature.

Studies based on idealized barotropic or baroclinic double-gyre ocean circulation models explain the decadal variability of the KE as the result of an intrinsic oceanic oscillation (Jiang et al., 1995; McCalpin and Haidvogel, 1996; Qiu and Miao, 2000; Dewar, 2003; Dijkstra and Ghil, 2005; Hogg et al., 2005; Pierini, 2006; Primeau and Newman, 2008; Gentile et al., 2018). In a nutshell, the mechanism in these models involves the accumulation of potential vorticity (PV) meridionally advected by the upstream Kuroshio current which, following PV conservation, generates large meanders of the KE that eventually block further PV advection. The reduced PV advection then straightens the KE path, enabling PV advection again to form a closed cycle.

Moreover, some studies favor the idea of wind-triggered intrinsic variability, in which the basin-scale wind variability and the resultant SSH anomalies in the form of Rossby waves trigger and pace the oceanic intrinsic processes that are usually of much larger amplitude than the wind-driven signal. The specific oceanic intrinsic processes involved, however, vary. Besides the PV advection/blocking mechanism just mentioned (Taguchi et al., 2007; Pierini, 2010, 2011, 2014; Zhang et al., 2017; Gentile et al., 2018), jet-topography interaction is also arguably a key oceanic intrinsic process. Particularly, Qiu and Chen (2005) proposed that the arrival of wind-driven SSH signals modulate the meridional position of the Kuroshio south of Japan, forcing it to flow passed the deep (shallow) segment of the Izu Ridge at 140°E, and the PV conservation generates

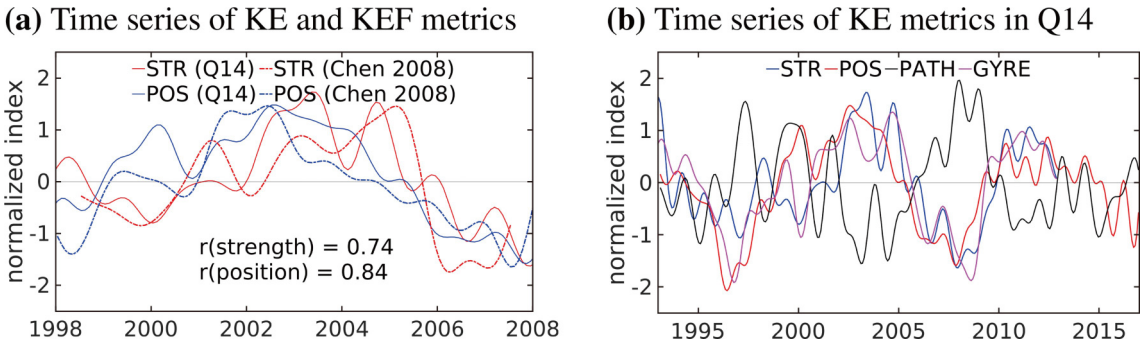

Fig. 2. (a) Time series of the strength (STR) and position (POS) indices of the KE (Q14) and the KEF (Chen, 2008). (b) Time series of the KE strength (STR), position (POS), path length (PATH), and recirculation gyre strength (GYRE) metrics from Q14. The time series are digitized from the respective references and then normalized about their respective mean and low-pass filtered with a cutoff period of one year.

stable (unstable) KE downstream to balance the vortex stretching (shrinking). Recent works by Qiu et al. (2020b) showed that the straight/meandering state of the Kuroshio south of Japan has the ability to modulate the KE state in the same way through the interaction with the Izu Ridge. Qiu and Chen (2010) put forth another theory attributing the KE decadal variability to wind-triggered jet migration and hence interaction with the deep (shallow) parts of the Shatsky Rise at 158°E, which induces suppressed (enhanced) mesoscale eddy activity that, with an adjustment time, feeds back upstream to the jet and brings it to its original latitude. Recently, Nonaka et al. (2020) used an ensemble 0.1° model experiment to quantify the relative importance of wind-driven and intrinsic variability in terms of KE jet speed and eddy activity. They found that on decadal timescales, the intrinsic/wind-driven ratios for jet speed and downstream (east of 153°E) eddy activity are both 0.73, and the ratio for upstream eddy activity is 2.73. It is thus inferable that wind-driven and intrinsic components of the KE decadal variability are both important, yet the exact mechanism concerning the respective roles of wind, jet, eddies, and topography, are still far from conclusive.

3. Midlatitude storm track dynamics and response to SST anomalies

Before reviewing research results on oceanic frontal impacts on the atmosphere, we first briefly introduce the dynamics of interaction between storm track and mean flow to lay the groundwork for the following discussions.

The westerly jet is one of the most salient features of the midlatitude tropospheric time-mean circulation (Fig. 3, contours). It is universally believed that two types of jets exist, namely the subtropical jet and the polar-front or the eddy-driven jet. Here, we do not differentiate between the two types in the context of this article, since in boreal winter, the two jets merge (Lee and Kim, 2003). The poleward flank of the westerly jet is where synoptic (2–8 days, or sometimes 1–10 days) variability associated with transient eddies (extratropical cyclones, or storms) is the most vigorous, often known as the storm track. In the upper troposphere, almost-circumglobal storm tracks exist in both hemispheres, while the lower-tropospheric storm track in the northern hemisphere is segmented by the continents into the North Pacific and North Atlantic parts. The storm track is commonly defined as the area with either the heaviest Lagrangian extratropical cyclone track density (Fig. 3a) or the strongest Eulerian synoptic variability (Fig. 3b) usually in terms of geopotential height, eddy heat flux, or eddy kinetic energy. The westerly jet and the storm track are dynamically interrelated, constantly in mutual adjustment (Chang et al., 2002), and can be described by the quasi-geostrophic storm track theory (Hoskins, 1983). According to the theory, a weakening to the jet forces anomalous baroclinic deformation of the transient eddies near the storm track exit, which shifts the storm track northeastward (from the eastern North Pacific to the western coast of Canada). The resultant negative vorticity deposition in turn drives a high-pressure anomaly to further weaken the westerly jet. In the meantime, the transient eddy vorticity deposition also emanates planetary Rossby waves (Hoskins et al., 1983; Sardeshmukh and Hoskins, 1988; Zhou et al., 2015) that propagate eastward along the jet, which acts as a waveguide (Hoskins and Ambrizzi, 1993; Branstator, 2002). Similarly, such mutual adjustment is also triggered when perturbations are initially made to the storm track.

Due to the interrelation between the time-mean flow and the storm track, SST-induced perturbations to each of them would cause a systematic atmospheric response. First, according to linear quasigeostrophic theory, the direct thermal response to surface sensible heating and mid-level latent heating induced by positive SST anomalies would exhibit a baroclinic structure with a near-surface low and an upper-level high (Hoskins and Karoly, 1981; Hendon and

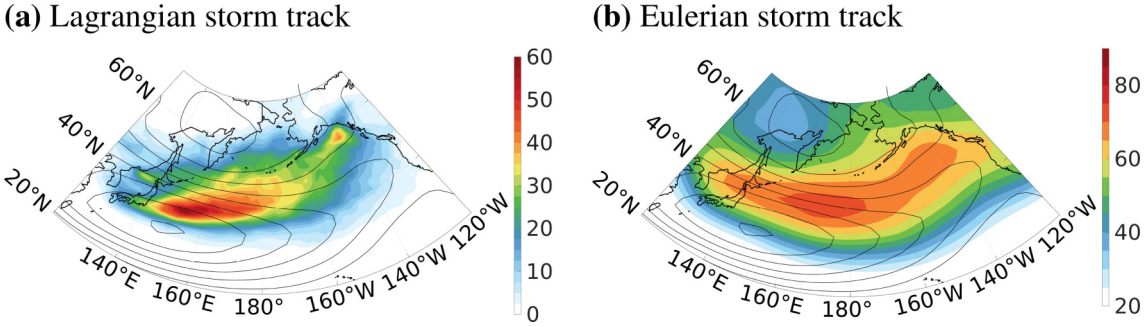

Fig. 3. (a) Lagrangian storm track defined as the track density of extratropical cyclones (number of cyclones in 2° × 2° grid boxes per winter, shading) during 1948–2011 overlaid on 1948–2018 mean zonal wind at 500 hPa (contours; CI = 5 m s^{-1}). Extratropical cyclone track data is developed by the Cooperative Institute for Climate and Satellites, North Carolina State University based on NOAA's 20th-century reanalysis dataset (https://etcsrv.cicsnc.org/ETCv8). Zonal wind data is from the NCEP-NCAR Reanalysis 1 dataset. (b) The 1948–2018 mean winter Eulerian storm track, defined as the standard deviation of 2-8-day bandpass filtered geopotential height (m, shading), overlaid on the zonal wind (contours; CI = 5 m s^{-1}), both at 500 hPa. Geopotential height and zonal wind data are from the NCEP-NCAR Reanalysis 1 dataset.

Hartmann, 1982; Frankignoul, 1985; Valdes and Hoskins, 1989; Ting, 1991; Ting and Peng, 1995; Peng and Whitaker, 1999; Hall et al., 2001). Dynamically, the heating is balanced by zonal and meridional cold air advection. In the steady state, dynamical feedback may alter the low-level response to the same sign as aloft, resulting in a barotropic structure (Kushnir et al., 2002; Smirnov et al., 2015). However, taking transient eddies into account, research (Ferreira and Frankignoul, 2005; Deser et al., 2007; Smirnov et al., 2015) has shown that the initial baroclinic thermal response modifies eddy activity and thus the convergence of eddy momentum, vorticity, and heat fluxes. In a time frame of 3 weeks to 4 months, eddy forcing quickly transforms the initial baroclinic response to an equivalent barotropic high with a downstream wavetrain (Peng et al., 1997; Peng and Whitaker, 1999; Kushnir et al., 2002). In this case, heating is balanced by eddy heat transport. See Fig. 4 for a schematic illustrating the thermally direct linear response and the eddy-mediated response (from Zhou, 2019). The eddy-mediated response to midlatitude SST anomalies has been extensively studied since the 1980s, first by means of modeling (Palmer and Sun, 1985; Ting and Peng, 1995; Kushnir et al., 2002; Zhou et al., 2015, 2017), and now confirmed by observational evidence (Liu et al., 2006, 2007, 2012a, b; Frankignoul and Sennéchael, 2007; Wang et al., 2010; Wen et al., 2010; Frankignoul et al., 2011a; Gan and Wu, 2013). This response, of course, is sensitive to the storm track background state in terms of position and strength (Peng et al., 1995, 1997; Peng and Whitaker, 1999; Walter et al., 2001; Zhou, 2019).

To understand the impacts of SST anomalies on the storm track, it is necessary to note the classic conceptual model of extratropical cyclone dynamics (Charney, 1947; Eady, 1949). It states that baroclinic instability of the time-mean flow is what triggers the cyclones and favors their development by converting mean flow available potential energy to eddy potential and kinetic energies. Therefore, the degree of mean flow baroclinic instability, or baroclinicity, especially near the entrance of the storm track, is a key parameter (Chang et al., 2002). Baroclinicity is usually measured by the Eady maximum growth rate (Eady, 1949; Lindzen and Farrell, 1980; Nakamura and Yamane, 2009), a parameter proportional to vertical shear of the horizontal wind (or, equivalently, the horizontal temperature gradient as per thermal wind balance), and inversely proportional to the static stability (or buoyancy frequency) of the atmosphere:

$$\sigma = 0.31 \frac{f}{N} \left| \frac{\partial \boldsymbol{u}}{\partial z} \right| = 0.31 \frac{g}{N\theta_0} \left| \left(-\frac{\partial \theta}{\partial y}, \frac{\partial \theta}{\partial x} \right) \right| , \tag{1}$$

where f is the Coriolis parameter, g is the acceleration of gravity, N is the static stability given by

$$N^2 = \frac{g}{\theta} \frac{\partial \theta}{\partial z} , \tag{2}$$

θ is the potential temperature, θ_0 is a reference temperature, and $\boldsymbol{u} = (u, v)$ is the horizontal wind vector. In a pure zonal flow, $\boldsymbol{u}$ reduces to the zonal component u and $\partial\theta/\partial x$ vanishes. For low-level baroclinicity, air-sea sensible heat flux is the dominant factor (Nakamura et al., 2004; Hotta and Nakamura, 2011), whereas latent heating dominates in the mid-troposphere (Hoskins and Valdes, 1990; Small et al., 2014; Tierney et al., 2018). The heat fluxes can alter both the horizontal temperature gradient and the static stability.

On the other hand, since the effect of extratropical cyclones is to transport heat poleward, they tend to weaken the temperature gradient and thus reduce baroclinicity, therefore hindering the development of subsequent cyclones. The very existence of storm tracks thus indicates that there must be a mechanism to restore the baroclinicity eroded by the destructive cyclones (Hoskins and Valdes, 1990). Besides the most fundamental source of baroclinicity—the equator-to-pole temperature difference (Chang et al., 2002; Marshall and Plumb, 2008), other sources of baroclinicity include quasi-stationary planetary waves generated by large-scale orography, and continent-ocean temperature contrast (Broccoli and Manabe, 1992; Lee and Mak, 1996; Brayshaw et al., 2009; Saulière et al., 2012). As will be seen below, ocean fronts and eddies can also maintain atmo-

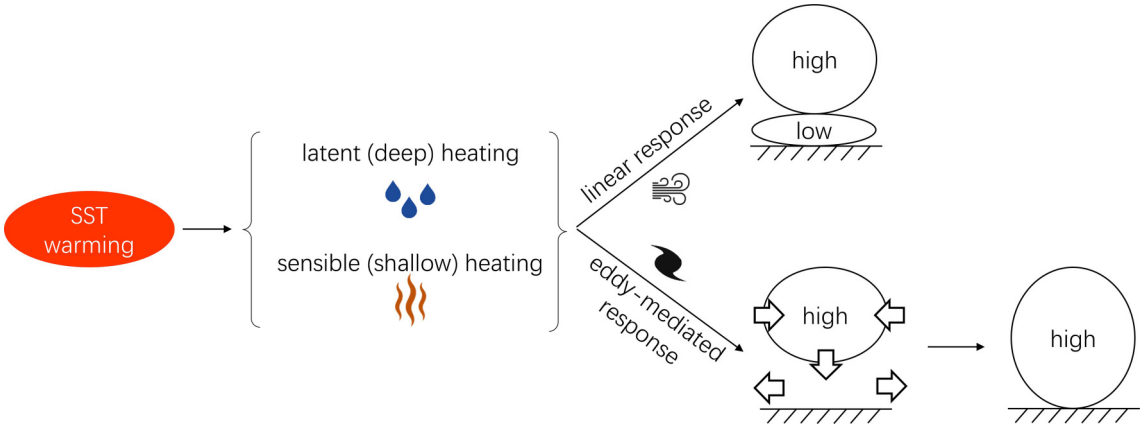

Fig. 4. Schematic showing the thermally direct, linear response and the eddy-mediated response to latent and sensible heating induced by large-scale SST anomaly in the KOE [Reprinted from Zhou (2019) with permission].

spheric baroclinicity through sensible and latent heating. See Fig. 5 for a schematic summary of chief baroclinicity sources for the storm track.

4. Impacts of oceanic fronts on the atmospheric mean flow

4.1. *Atmospheric time-mean response to SST frontal forcing*

Midlatitude SST fronts can drive anomalous low-frequency or time-mean atmospheric flow. The SST frontal forcing to the atmosphere is first "felt" by the marine atmospheric boundary layer (MABL) immediately above the sea surface, whose perturbations then drive the free-atmospheric response aloft. The midlatitude MABL can, on the first order, be described by the Ekman balance:

$$f\boldsymbol{k}\times\boldsymbol{u} = -\frac{1}{\rho_0}\nabla p + \boldsymbol{\tau}\,, \tag{3}$$

where f is the Coriolis parameter, $\boldsymbol{k}$ is the vertical unit vector, $\boldsymbol{u}$ is the horizontal wind, ρ_0 is a reference air density, ∇ is the horizontal gradient operator, p is the pressure, and $\boldsymbol{\tau}$ is the wind stress. To account for the influence of the oceanic front, Feliks et al. (2004) proposed an idealized dry MABL model, in which the MABL air is assumed to be well-mixed and have the same temperature as the SST. In this sense, pressure is solely controlled by SST via the hydrostatic equation as $\nabla\partial P/\partial z = \rho_0 g\nabla T/T_0$. The stress is given by $\boldsymbol{\tau} = K(\partial^2\boldsymbol{u}/\partial z^2)$, where K is the eddy diffusivity coefficient. From this model, Feliks et al. (2004) derived a vertical wind velocity at the top of the MABL that contains two terms:

$$w = \gamma\nabla^2\psi - \alpha\nabla^2 T\,, \tag{4}$$

where ψ is the horizontal streamfunction of the large-scale flow above the MABL in the free atmosphere, T is SST, ∇^2 is the Laplacian operator, and α and γ are constants. The first term (namely the mechanical term) represents Ekman pumping due to surface friction, acting to damp the large-scale vorticity via vortex stretching, and the second term (namely the thermal term) accounts for the impact of SST on surface pressure via hydrostatic balance, which is responsible for driving the quasigeostrophic circulation aloft. Therefore, the thermal forcing by the oceanic front drives an anticyclonic (cyclonic) vortex with updraft (downdraft) over the warm (cold) flank of the front up to the tropopause level. The two thermally induced free-atmospheric vortices then spin up a jet in between, parallel to the front. This theoretical response was reproduced in both an idealized dry barotropic model (Feliks et al., 2004) and a two-mode baroclinic one (Feliks et al., 2007). The atmospheric response in this model also exhibits barotropic and baroclinic instabilities when the SST front is as strong as the realistic Gulf Stream and Kuroshio fronts. The instability waves have dominant periods of 1–7 months. This model was successful in realistically representing interannual atmospheric variability when forced with observed high-resolution SST (Feliks et al., 2011). Further analysis by Brachet et al. (2012) using a high-resolution (0.5°) atmospheric general circulation model (AGCM) favors this mechanism. They also found that the thermal term of the atmospheric response dominates in the long-term mean, and the mechanical term becomes equally important for the process of Ekman pumping on 10-day timescale. Decreased (increased) stability and increased (decreased) cloud cover are also observed on the warm (cold) flank of the front.

Minobe et al. (2008) put forth a similar hydrostatic MABL model for the midlatitude SST frontal zones, where the stress term is simply written as $\boldsymbol{\tau} = \varepsilon\boldsymbol{u}$, ε being a constant frictional damping coefficient, noting further that the surface pressure is also forced by SST but is barotropic:

$$\varepsilon p + H\left(\frac{\partial u}{\partial x} + \frac{\partial v}{\partial y}\right) = -\gamma\,, \tag{5}$$

where H is the depth of the MABL. This model is based on that of Lindzen and Nigam (1987) for the tropics. The long-term MABL response is similar to the Feliks et al. (2004, 2007) model, characterized by low-level convergence over warm SST and divergence over cold SST (Fig. 6). The result-

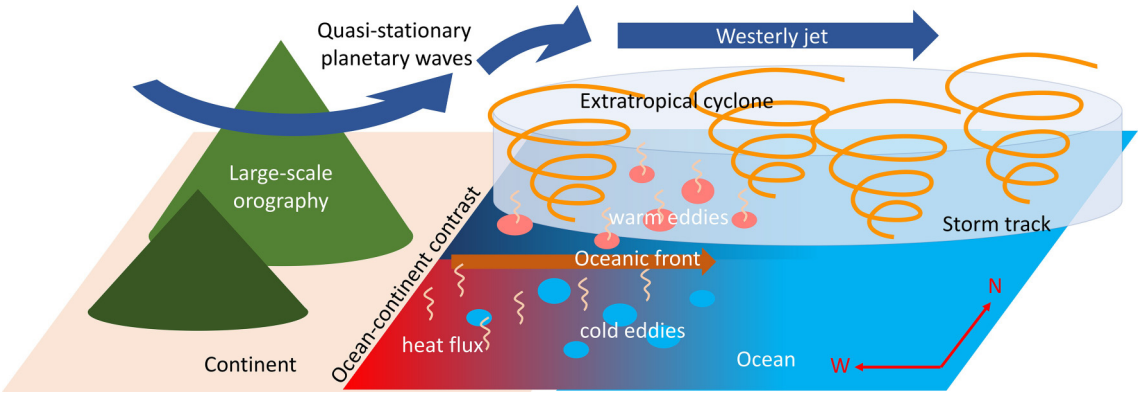

Fig. 5. Schematic showing the main sources of baroclinicity: the quasi-stationary planetary waves generated by large-scale orography, the ocean–continent contrast, and the oceanic fronts and eddies.

ant ascent over the warm flank maximizes just above the MABL and penetrates through the whole troposphere. In this case, it could be easily derived that the MABL convergence is proportional to the Laplacian of pressure and SST, which are subsequently confirmed by several studies using satellite observations and AGCMs (Bryan et al., 2010; Kuwano-Yoshida et al., 2010; Minobe et al., 2010; Shimada and Minobe, 2011), thus favoring the Minobe et al. (2008) model. Similar findings are also obtained for the KE front in the North Pacific (Nonaka and Xie, 2003; Taguchi et al., 2009; Xu et al., 2011; Sasaki et al., 2012), the Agulhas Current in the Southern Ocean (O'Neill et al., 2003, 2005; Nkwinkwa Njouodo et al., 2018), and the Brazil-Malvinas Currents in the South Atlantic (Tokinaga et al., 2005). In the above studies, a band of increased high cloud and intense convective precipitation is also commonly found collocated with the warm SST from satellite observations and are attributed to the reduced stability and enhanced evaporation, although the model itself is dry. The Minobe et al. (2008) model was based on annual-mean conditions, and Minobe et al. (2010) further discussed its seasonality. It was shown that in winter the atmospheric response to the ocean front is characterized by a shallow heating mode associated with surface wind convergence, while in summer a deep heating mode was found to be driven by deep convection and moisture advection. It is argued that two conditions are necessary for the deep heating mode: SST of 24°C–26°C, and moisture transport from lower latitudes, which can both be present in the KE region too.

The MABL models proposed by Feliks et al. (2004, 2007) and Minobe et al. (2008) are both based on the Ekman balance and the hydrostatic pressure adjustment to SST forcing, and are therefore commonly known as the "pressure-adjustment mechanism". Lambaerts et al. (2013) performed an idealized modeling experiment to evaluate the two MABL models, using a vertically sheared background wind of 1 m s^{-1} at an altitude of 1200 m. Under such weak wind conditions, the two models were found to be reasonably good approximations to the real MABL. However, both models are insensitive to the magnitude and relative direction of the background wind regarding the SST front. Kilpatrick et al. (2014) employed an idealized dry setup of the WRF regional atmospheric model to show that in the case of strong cross-frontal wind (~10 m s^{-1}), changes of turbulent mixing and MABL height across the front result in depth-integrated convergence when the wind blows from the cold side to the warm side, and that the surface wind convergence is of the opposite sign of the depth-integrated convergence, indicating that the mixed-layer assumption breaks down. The effective timescale of an air column crossing the front is shorter than an inertial period, therefore the MABL temperature and pressure adjust to SST anomalies over a longer length scale than the turbulent stress term. Thus the MABL response over the front is governed by increased (decreased) downward momentum transfer by enhanced (reduced) turbulent mixing over the warm (cold) SST. This mechanism is known as the "vertical mixing mechanism" (Wallace et al., 1989). Aloft, however, the SST front excites an inertia-gravity wave which is unable to influence the free-atmospheric circulation in this dry setup. In the realistic moist atmosphere, a free-atmospheric response driven by enhanced latent heating is nevertheless possible. Based on the same idealized framework as Kilpatrick et al. (2014), Kilpatrick et al. (2016) further showed that under along-frontal wind conditions, the free-atmosphere response conforms to the pressure adjustment mechanism, and its magnitude increases with the background wind. Using realistic reanalysis data for mid-winter, Masunaga et al. (2020a) showed that the hydrostatic pressure adjustment is at work over the KE, where surface winds are more parallel to the SST front, but the vertical mixing mechanism is responsible for the time-mean divergence near the OE, where monsoonal surface winds cross the SST front perpendicularly. For the Gulf Stream and Agulhas Return Current frontal regions, Masunaga et al. (2020b) proposed that vertical mixing is the main mechanism.

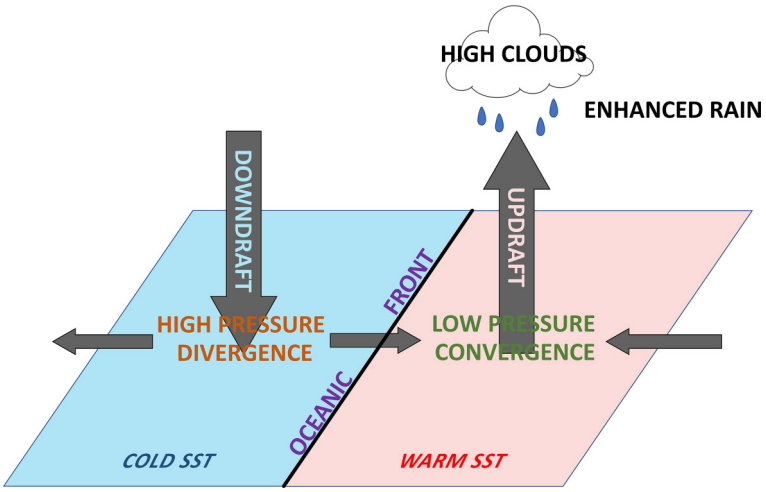

Fig. 6. Schematic showing the atmospheric mean-flow response to a mid-latitude SST front (see section 4.1).

4.2. *Relationship between the mean-flow and transient eddy responses*

The above discussions on MABL and free-atmosphere responses to SST fronts are restricted to the context of the steady-state or long-term mean. The midlatitude atmosphere, however, is dominated by energetic transient (synoptic) weather systems organized in the storm track which effectively mask any steady-state feature. Considering this, the mean-flow response to SST fronts is usually extracted by taking a monthly, seasonal, or annual average, which implicitly relies on the assumption that the high-frequency fluctuations caused by transient eddies can be largely canceled out (i.e., with zero time-mean) over a sufficiently large number of samples. However, recent studies started questioning this assumption. Parfitt and Czaja (2016) demonstrated that over the Gulf Stream front, synoptic variability is present about 95% of the time, and the time-mean precipitation and vertical wind along the warm flank of the front are largely set by the residual of averaging over the cyclones and anticyclones. Particularly, the vertical wind, a quantity taking both positive and negative signs, does not cancel out when averaged. More specifically, adiabatic ascent and descent due to isentropic upglide and downglide (Hoskins et al., 2003) do compensate to a large degree, but the diabatic contribution to upward motion, which is concentrated in a small part in the extratropical cyclone's fronts where condensation takes place (see Fig. 7 for a schematic of typical extratropical cyclone structure), is not compensated by the downward motion found in the trailing anticyclone because the descending air there has other origins. Averaging over many cyclones and anticyclones, the net vertical motion is upward and maximized along the oceanic front. In line with this, O'Neill et al. (2017, 2018) confirmed that surface convergence anomalies under stormy conditions are 1–2 orders of magnitude larger than the climatological mean and that they indeed have a highly asymmetric distribution skewed toward convergent winds. Removing either a small number of rainfall events or extreme convergence events (these two are equivalent, see Plougonven et al. (2018)) associated with storms effectively removes the time-mean convergence zone, leaving a time-mean divergence field that cannot be explained by the Ekman-balanced MABL models. These analyses suggest that the time-mean convergence and upward motion seen in observations are insufficient to indicate the frontal impact on the atmospheric mean flow—they could well be the rectified manifestation of the SST front's anchoring effect on the storm track. Even if an SST-frontal driven mean-flow response does exist, it is certainly overshadowed by the storm track response, and therefore a much more carefully designed technique than a straight time-mean must be employed to isolate it.

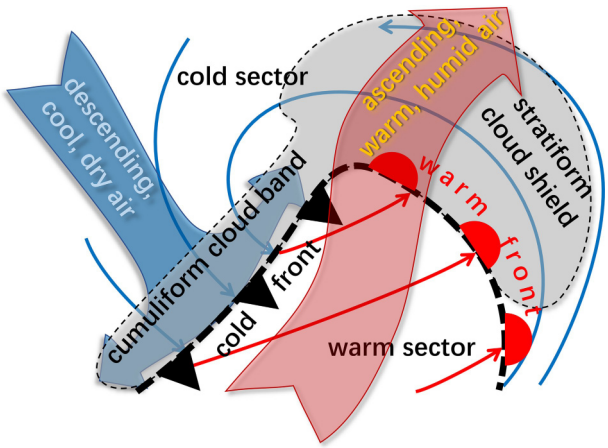

Fig. 7. Schematic of the structure of an idealized extratropical cyclone during its mature phase, showing the cold and warm air flows (thin arrowed curves), the cold and warm fronts (black dashed curve with black triangles and red semicircles), the cloud cover (grey shading), and the cold and warm conveyor belts (faded blue and red block arrows). Based on Bjerknes and Solberg (1922) and Stull (2017).

Recent works started analyzing the storm-free, mean-flow response to oceanic fronts using more sophisticated physics-based methods. It is found that the condensation-induced vertical motion found primarily in the atmospheric fronts (mostly cold fronts) of extratropical cyclones significantly contributes to the time-mean updraft zone, which is suggestive of the importance of the atmospheric frontal (mesoscale) response to oceanic fronts (also mesoscale). At least for over the Gulf Stream region, atmospheric fronts occur only ~22%–25% of the time near the oceanic frontal zone (Parfitt et al., 2016; Masunaga et al., 2020b), yet they are responsible for 90% of the precipitation (Catto et al., 2012; O'Neill et al., 2017), which is associated with convergence and updraft. In light of this, Parfitt and Seo (2018) performed atmospheric frontal detection and confirmed that frontal events dominate the climatological surface convergence. Analyzing only the non-frontal conditions over both the Gulf Stream and KE frontal regions, they found that the non-frontal divergence is generally weaker than non-frontal convergence in magnitude but occurs more frequently (70%–85% vs. 15%–30%), thus setting the weak, storm-free, time-mean divergence found by O'Neill et al. (2017, 2018). This indicates that if the Ekman-balanced pressure adjustment response to SST fronts does indeed exist, its surface convergence shall work to increase non-frontal convergence so that it cancels more exactly with non-frontal divergence in the time-mean, resulting in a weak signal. More recently, Masunaga et al. (2020a) further showed that for the KOE region in mid-winter, moderate-strength convergence mostly shapes the time-mean convergence pattern around the SST front, while extreme events account for a large portion but in a spatially homogeneous manner. Specific processes corresponding to the moderate-strength convergence events include stationary atmospheric fronts, generation of meso-α cyclones and surface troughs, and the passage of synoptic-scale cyclones. Similar results are found for the Gulf Stream, but very weak for the Agulhas Return Current (Masunaga et al., 2020b).

The recent debate over the time-mean convergence and precipitation bands along the midlatitude oceanic fronts

reflects the complexity of the midlatitude air-sea interaction owing to the powerful synoptic transient atmospheric eddies that often respond more vigorously to SST perturbations than does the mean-flow. It, therefore, calls for a more in-depth investigation on the SST frontal influence on extratropical cyclones, especially regarding their mesoscale structures (atmospheric fronts and cold and warm sectors), as well as their statistics, i.e., the storm track. Moreover, considering the overwhelming storm influence on the atmospheric general circulation, observed time-mean results previously regarded as evidence for the mean-flow response to oceanic fronts must be carefully re-interpreted. Particularly, the situation when storm influence is less dominant, e.g., during summer or at the subtropical Gulf Stream and Kuroshio fronts, would likely provide more insights into the problem of atmospheric mean flow response. For instance, Miyama et al. (2012) noticed a rain band that persisted for two days in May in the vicinity of the Kuroshio front in the East China Sea using radar observations, and also successfully simulated the rain band in a 3-day regional model integration. Since there was no extratropical cyclone passing by, and the seasonal Baiu/mei-yu front is far to the north, the rain band was regarded as evidence for the Minobe et al. (2008) model. Whether this 2–3-day signal could represent the typical storm-free and atmospheric front-free mean-flow response to the oceanic front, and whether the results hold for the KE region, are still open questions. Moreover, the summertime-mean response such as presented in Minobe et al. (2010) could presumably better reflect mean-flow response than winter-mean, thanks to weaker extratropical storm activity in summer, but whether and to what extent this is true is unknown.

5. Importance of oceanic fronts to storm tracks

5.1. *Influence on storm structure and development*

Extratropical cyclones have been the centerpiece of meteorological research for decades [see Schultz et al. (2019) for a comprehensive review]. The role of the warm western boundary currents in cyclone genesis and development has also long been acknowledged. For example, studies have shown that the large upward sensible and latent heat fluxes from the sea surface facilitate cyclone development by enhancing both its warm conveyor belt (Booth et al., 2012) and cold conveyor belt (Hirata et al., 2015, 2016, 2018). However, the role of oceanic fronts, i.e., the sharp SST gradient, on extratropical cyclones has not received extensive research interest until recent years. Following the highlight on the importance of atmospheric frontal response to SST fronts in setting the time-mean response (see above) by Parfitt and Czaja (2016), they went on to examine the influence of the Gulf Stream fronton atmospheric frontal activity using an AGCM. Their results confirmed that the strong SST front indeed enhances atmospheric frontal development by ~30%.

Besides atmospheric fronts, oceanic frontal impacts on other mesoscale components of extratropical cyclones have also been recently examined. Using a regional model, Vannière et al. (2017a) studied the response of a single extratropical cyclone to the Gulf Stream front, showing that for a single cyclone, a band of precipitation and surface convergence is reproduced and that the precipitation response is dominated by anomalous convective precipitation in the cold sector of the storm. The same authors also analyzed extratropical cyclones in the ERA-Interim reanalysis (Vannière et al., 2017b), and found that cold sector precipitation is confined to a narrow band south of the Gulf Stream front, while precipitation outside the cold sector distributes over a broader area, suggesting that a large part of the anchoring effect of the SST front on precipitation is through the cold sector. Since strong upward motion is also seen outside the cold sector (it is maximized along the cold front), a direct link between the ascent and the precipitation responses to the oceanic front seems unlikely. However, cold sector convection can steepen the isentropic surfaces by means of diabatic heating (Papritz and Spengler, 2015), which can force stronger adiabatic ascent in the warm sector of subsequent cyclones. There is also an AGCM study on the influence of the oceanic front on the warm sector of extratropical cyclones by Sheldon et al. (2017), who examined the origin of the ascent in the warm conveyor belt of an individual extratropical cyclone by back-tracing the trajectories of air parcels in the core of the ascending motion to their initial location 24 hours prior. Comparing the backward-trajectories in a control experiment with a realistic oceanic front and a sensitivity experiment where the front is smoothed, it was found that the warm SST to the south of the front maintains a high equivalent potential temperature for those air parcels initially traveling at low levels along the current and thus favoring their ascent, which is reinforced by a thermally direct secondary circulation driven by the SST gradient. This is further confirmed by analyzing the ERA-Interim dataset.

5.2. *Influence on storm track maintenance*

As introduced in section 3, the existence of midlatitude storm tracks requires a source to restore the baroclinicity eroded by eddy mixing. Nakamura et al. (2004) proposed that the sensible heat flux contrast across midlatitude oceanic fronts is an important source of low-level baroclinicity, through which the fronts "anchor" the storm track. Making use of an aqua-planet model setup, Nakamura et al. (2008), Nonaka et al. (2009), and Sampe et al. (2010) found that the cross-frontal sensible heat flux contrast is capable of restoring near-surface baroclinicity within 2–3 days after a cyclone passes by, and this process is termed the "oceanic baroclinic adjustment". Recent work by Vannière et al. (2017b) based on reanalysis data further confirmed this finding. It is also found by the aqua-planet modeling studies that if the front is removed, the strength of the low-level storm track would plunge by 70%–75%, and the upper-level storm

track would halve. However, in an aqua-planet, due to the absence of continent-ocean contrast and orographically generated quasi-stationary waves, the role of oceanic fronts could have been exaggerated. Indeed, the AGCM study by Inatsu and Hoskins (2004) argued that albeit the contribution of oceanic fronts to low-level storm track is strong, its contribution to upper-level storm track is only mild. Other modeling studies (Wilson et al., 2009; Brayshaw et al., 2011; Kaspi and Schneider, 2013) argued that oceanic fronts only contribute secondarily to baroclinicity and storm track, compared with continent-ocean contrast and quasi-stationary waves. These studies, however, used rather crude grid resolution (1.5°–3°) and therefore are subject to a severe underestimation of the impacts of oceanic fronts.

Using a high-resolution (0.5°) regional model, Taguchi et al. (2009) found that the existence of the KOE fronts plays a key role in simulating a North Pacific storm track with realistic strength and position and that removing the fronts would weaken the low-level storm track by 15%–20% and shift it to the south. Woollings et al. (2010) used a similar high-resolution (50 km) regional model to prove that the existence of the Gulf Stream front in the North Atlantic pushes the storm track into the interior of the ocean basin, otherwise it would be largely trapped along the coastal zone by the dominant control of continent-ocean contrast. Further, using a 0.5°-resolution AGCM, Small et al. (2014) confirmed the key role of Atlantic and Southern Ocean fronts by quantitively assessing the contribution of oceanic fronts to low-level storm track. It was shown that local contribution reaches as high as 20%–40%, while the average contribution over the entire storm track region is about 10%–20%. Recently, Kuwano-Yoshida and Minobe (2017) compared the storm track between AGCM experiments (50 km resolution) with and without the KOE fronts, and found that the existence of the KOE fronts increases the frequency of explosive extratropical cyclones in the North Pacific, shifts the westerly jet northwards, and leads to more precipitation over the western coast of North America. Summarizing the current findings, it is now safe to state that oceanic fronts are indeed a significant factor for the maintenance of the storm track, contributing ~20% at low levels and less at high levels.

5.3. *Response of storm track to changes of SST fronts*

A few studies investigated the atmospheric impacts of oceanic fronts with changing strength and position, taking advantage of idealized model experiments. Aqua-planet modeling results of Ogawa et al. (2012) and Deremble et al. (2012) suggest that the storm track migrates meridionally following the meridional shift of the midlatitude oceanic front, but when the front has moved to subpolar latitudes, the storm track does not follow it anymore, instead appears back at the midlatitudes. Also using an aqua-planet model, Michel and Rivière (2014) further noticed that the westerly jet and the storm track both intensify with stronger, wider, and southerly displaced oceanic fronts. The idealized but non-aqua-planet AGCM study by Graff and LaCasce (2012) revealed that an enhanced SST gradient and an increase in absolute SST can both strengthen the storm track and shift it northward. Yao et al. (2016) used a regional model and gradually increased the SAFZ SST (positively correlated to the position of the OEF) in a series of experiments, and found that the storm track strengthens and moves to the ocean interior, and its meridional extent becomes narrower. More recently, Foussard et al. (2019) confirmed the meridional shift of the storm track following the oceanic fronts, using an idealized regional model. The above results commonly support the idea that the storm track strength and position are controlled by the midlatitude oceanic front.

5.4. *Relative roles of the absolute SST and SST gradient*

However, there are still disputes over the relative roles of the sharp SST gradient across the front and the high absolute SST to the south of it. The former, as discussed above, favors storm development by means of increasing lower-level baroclinicity, and has received extensive modeling support (Taguchi et al., 2009; Sampe et al., 2010; Woollings et al., 2010; Hotta and Nakamura, 2011; Graff and LaCasce, 2012; Révelard et al., 2016) and observational validation (Vannière et al., 2017b). The latter, on the other hand, enhances the storm track by supplying enormous latent heat, adding to mid-level baroclinicity (Stoelinga, 1996; Businger et al., 2005). It can also reduce atmospheric static stability and thus enhance downward turbulent momentum transfer (Booth et al., 2010; Liu et al., 2013). Recently, De Vries et al. (2019) performed sensitivity experiments to a single extratropical cyclone and found that the latent heating associated with high absolute SST can better favor the cyclone development than the SST gradient. This argument is supported by sensitivity experiments of Small et al. (2019), who additionally indicated that besides latent heating, the absolute SST can also change the continent-ocean temperature contrast, and is therefore a greater factor in affecting the storm track than the SST gradient. However, as admitted by Small et al. (2019), their results are very sensitive to the storm track metrics. Furthermore, some modeling and reanalysis studies take the view that the two mechanisms are equally important (Sheldon et al., 2017), or that their relative importance depends on the SST anomaly—if the SST decreases more to the northern flank of the front than it increases to the south, then the positive contribution of the intensified SST gradient to the Eady growth rate could be offset by the enhanced static stability (Kuwano-Yoshida and Minobe, 2017). Clearly, more investigations are needed to better resolve this issue.

6. Decadal modulation of KOE fronts on the atmosphere

Given the above findings, it is interesting to investigate the impacts of the decadal fluctuation of KOE fronts on the North Pacific storm track, especially knowing that the anomalous storm track could further bring forth significant

responses of the atmospheric time-mean flow. Several observational studies and a few modeling studies have examined this issue, yet their results show large controversy. Here, we review the current progress by first remarking on some of the common issues concerning observational studies.

6.1. *Remarks on observational studies*

Observational studies are subject to several kinds of difficulty and uncertainty. (1) First, many observational studies rely on atmospheric reanalysis data, yet currently available datasets often use low-resolution SST data as boundary forcing to their models and can therefore heavily underestimate the oceanic frontal impacts on the atmosphere. Although data assimilation could remedy this issue to some extent, its effectiveness is uncertain. The fidelity of such research results is thus compromised. This issue was first raised by Frankignoul et al. (2011b, hereafter F11) based on the 2.5°-resolution NCEP-NCAR Reanalysis-1 data. Another widely used reanalysis dataset—the ERA-Interim data—underwent several resolution enhancements of the prescribed SST (1°→0.5°→0.05°) (Dee et al., 2011). Since the resolution of the atmospheric model remained 0.75°, the effective SST refinement is actually 1°– 0.75°. This has immense impacts on atmospheric quantities including the storm track (Masunaga et al., 2015; Parfitt et al., 2017; Zhang et al., 2020a). Smirnov et al. (2015) examined the influence of the OEF's meridional shift on the atmosphere using both NCEP-NCAR (2.5°) and ERA-Interim (0.75°) and found that the atmospheric response detected in ERA-Interim is 40% stronger than in NCEP-NCAR, suggesting the significance of increased SST resolution. However, using the same NCEP-NCAR dataset and the ERA-Interim on a 1.5° grid, Révelard et al. (2016) found a basically similar atmospheric response to KE bimodal variability and therefore concluded that data assimilation can indeed effectively compensate the effects of crude resolution. This argument, however, does not rule out the possibility that the frontal signature in both datasets is underestimated. (2) Second, since the atmospheric response to midlatitude SST anomaly has proven to be very sensitive to the background atmospheric state (Peng et al., 1995, 1997; Ting and Peng, 1995; Peng and Whitaker, 1999; Okajima et al., 2014), studies focusing on different time periods could yield vastly different results, especially under climate regime shift or climate change conditions where background atmospheric circulation and storm track change dramatically (Yin, 2005; Lu et al., 2010; Wu et al., 2011; Gan et al., 2017). Hence, results based on different time periods must be compared with caution. (3) Third, because the ocean and atmosphere are in constant interaction, any observed state is a mixture of forcing and response, as well as external remote influences such as from ENSO (Kelly and Jones, 1996). It is therefore necessary to rely on statistical methods to separate atmospheric response to atmospheric forcing and external signature. Many widely used methods (Frankignoul et al., 2011a; Liu et al., 2012a, b), including the maximum covariance analysis and the lag-correlation analysis, are built upon an assumption about the atmospheric response delay, that is, the time needed for the atmosphere to fully adjust to the SST anomaly (Frankignoul et al., 2011a; F11 hereafter). The atmospheric response delay was estimated from 3 weeks to 4 months (Ferreira and Frankignoul, 2005; Deser et al., 2007; Smirnov et al., 2015), and is commonly taken as 2 months in recent studies (e.g., Révelard et al., 2016). However, this value is purely empirical, and the atmospheric response has been shown to be very sensitive to it (F11; Smirnov et al., 2015). Other methods, such as synchronous correlation or composite analysis, simply cannot separate forcing and response, and their results are thus hard to interpret. External forcing is typically assumed to be from ENSO in the tropical Pacific and can be removed using linear regression models. However, the different ENSO-removal methods could introduce extra differences in the results. External forcing from other regions and processes, such as the Aleutian-Icelandic Seesaw (Honda and Nakamura, 2001; Honda et al., 2001, 2005), could also be at work but are usually ignored. Hence, observational studies must be carefully performed and interpreted.

6.2. *Impacts of KE bimodal variability*

The very few existent observational studies on atmospheric impacts of the KE bimodal variability are summarized in Table 1. These studies used various definitions of the KE mode index. F11, to our knowledge, is the first research in English literature to directly examine the impacts of KE or KEF decadal variability on the atmosphere. They defined the KE index as the leading principal component (PC) of the latitude of the 14°C isotherm at 200 m below the sea surface between 142°–160°E, using the World Ocean Database 2005 spanning 1979–2007. O'Reilly and Czaja (2015) defined the KE mode index using the maximum covariance analysis method, which involves performing a singular value decomposition on the covariance matrix of the SST gradient and geostrophic velocity (or SSH gradient) anomalies to detect a time series maximizing the covariability of both the dynamic and thermodynamic aspects of the KE. The positive phase of the resultant KE index corresponds to the stable mode of KE, and vice versa. Originally, the index was obtained from the AMSR–AVHRR blended SST and AVISO SSH satellite dataset for 2002–2011 and was then projected back to 1992 based solely on SSH. Révelard et al. (2016) used the KE bimodal index of Qiu et al. (2014, hereafter Q14), which is defined as the SSH anomaly averaged in the region 31°–36°N, 140°–165°E, i.e., the region of the southern recirculation gyre south of the KE. This index is in very high correlation with a more sophisticated synthesized index defined as the average of four normalized time series: the latitude of upstream (west of 153°E) KE, its path length reversed, its strength represented by the SSH difference across the axis, and the strength of the southern recirculation gyre. The advantage of the SSH-based index is that it is much easier to calculate. By this definition, a positive KE index signifies a stable KE. Zhang and Luo (2017) made use of the Luo et al. (2016) index, defined as the difference of the aver-

age SSH between two 3°-latitude boxes north and south of 35°N in the upstream KE area. This index, termed the KE dipole index, is by definition similar to the KE strength index which is one of the ingredients of the Q14 mode index. It is shown to represent the variability of the upstream KE meanders and mesoscale eddies, with the positive mode associated with the case of small meanders and reduced eddy kinetic energy, i.e., the stable mode of KE. A comparison of the four indices is shown in Fig. 8a.

The atmospheric impacts of the KE decadal variability found in literature studies, as indicated by Table 1, are vastly disparate. Révelard et al. (2016) speculated that the reason their results differ from those of F11 may be because the Q14 index they used is a synthesized index having variab-

Table 1. Observational studies on KE bimodal variability impacts on the atmosphere.

Reference	Index	Index area (°N, °E)	Time range	Dataset and resolution	Storm track response	Circulation response
Frankignoul et al. (2011b)	lat[T14$_{200}$]$_1$	—, 142–160	1980–2008	NCEP 2.5°	—	Kamchatka high, KE low
O'Reilly and Czaja (2015)*	SVD[SST, SSH]	32–37, 135–155	1992–2011	ERA-Interim 0.75°	west +, east –	quadruple over NP
Révelard et al. (2016)	SSH	31–36, 140–165	1979–2012	ERA-Interim 1.5°	downstream +	NP high, Alaska low
Zhang and Luo (2017)*†	SSH DIFF	32–35/35–38, 141–153	1993–2015	NCEP 2.5°	–↑	downstream jet ↑

Note: T14=14°C isotherm; □$_{200}$ = at 200 m depth; □$_1$ = PC1; lat = latitude; ↑ = northward shift; + = strengthening; – = weakening; — = not shown. * indicates that the study used synchronous correlation or composite analysis. † indicates that the study did not remove external forcing from ENSO or prove it small. Zhang and Luo (2017) used the SSH difference between areas south and north of 35°N, which are shown separately in the third column.

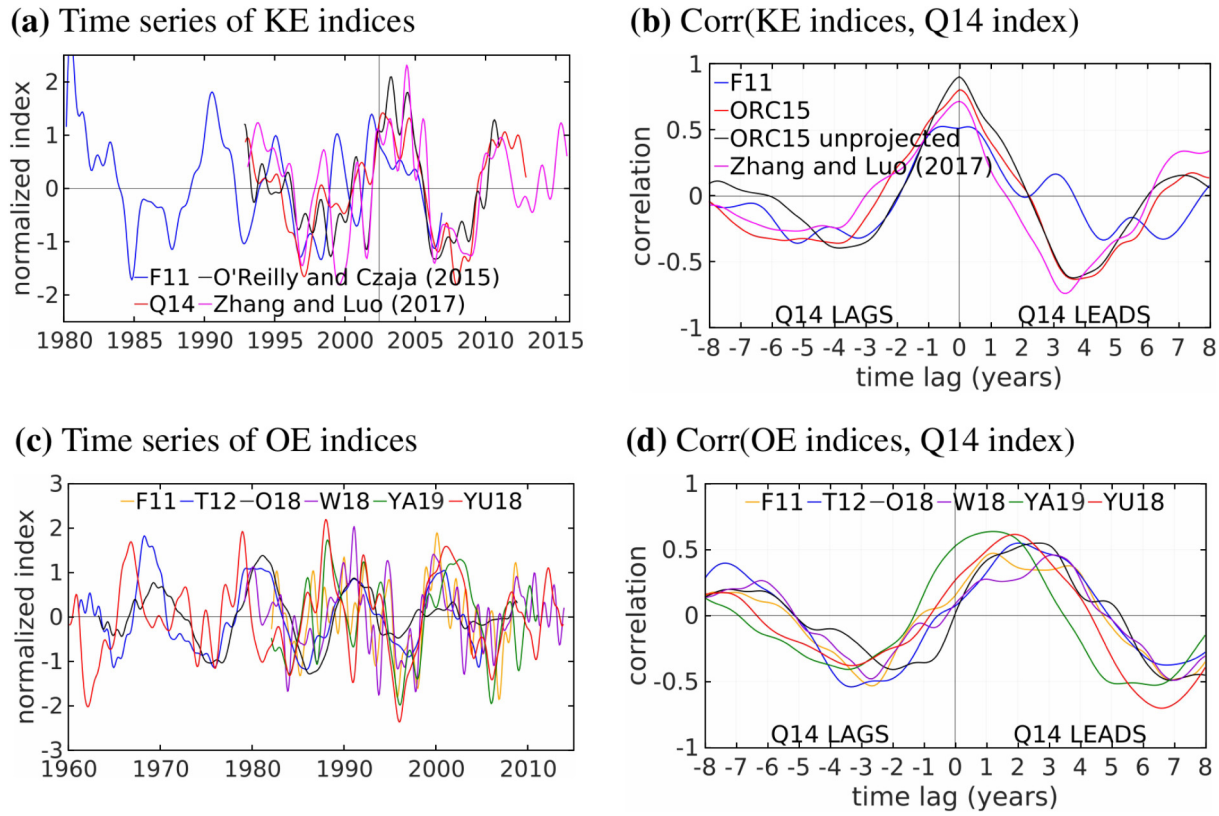

Fig. 8. (a) Time series of KE indices from various literature studies indicated in the legend. The vertical line denotes June 2002, before which the O'Reilly and Czaja (2015) index is projected backward using SSH data. (b) Cross-correlation between the literature KE indices and the Q14 index, with the full (projected) and unprojected indices of O'Reilly and Czaja (2015) shown separately. (c) Time series of OE indices from various literature studies indicated in the legend. References: T12: Taguchi et al. (2012); O18: Okajima et al. (2018); W18: Wills and Thompson (2018); YA19: Yao et al. (2019); YU18: Yuan and Xiao (2018). Here, the Taguchi et al. (2012) index is shown as the winter (DJF) mean of the authors' monthly indices. Yuan and Xiao (2018) provided indices for each season. Shown here is their winter index. (d) Cross-correlation of literature OE indices with the Q14 KE index. Indices are digitized from the respective references and then normalized about their respective mean and low-pass filtered with a cutoff period of one year.

ility of its four ingredients blended, whereas the F11 index solely represents the meridional shift of the temperature front. In fact, this argument is also relevant when comparing the Révelard et al. (2016) results with those of Zhang and Luo (2017). However, the effectiveness of this synthesized-versus-solo-index argument to explain the different atmospheric impacts is arguably limited, noticing that the Q14 synthesized index bares a high correlation with each of its ingredients (not shown), and with the KE strength index of Zhang and Luo (2017; Figs. 8a, b). The KE index of F11, in fact, is only moderately correlated with that of Q14 during their overlapping period (Fig. 8b). A more valid reason could be that the F11 index is just the leading PC, instead of full variability, and that it is defined by 200 m temperature, a relatively shallow level to define the deep-reaching KE jet and may not be fully representative of its position. Previous studies on the KE dynamics have commonly chosen a deeper level, e.g., the 12°C isotherm at 300 m used by the pioneering work of Mizuno and White (Mizuno and White, 1983). The index of F11 exhibits smaller meridional migration than the SSH-based KE position indices. Further, Révelard et al. (2016) noticed that the original un-projected bi-factor (SST and SSH) index of O'Reilly and Czaja (2015) is very similar to the Q14 index, yet the similarity is lost after the index is projected back to 1992 based on SSH data alone. Révelard et al. (2016) verified that using only the un-projected index results in similar atmospheric impacts with the Q14 index, yet the time series is too short to allow for statistical significance. We notice, however, that while the correlation between the projected index and the Q14 index is indeed lower than the un-projected (0.9), it is still as high as 0.8 (Fig. 8b). Therefore, whether this subtle difference is actually responsible for the contradicting atmospheric impacts is doubtful. Last, as stated above, the crude resolution of atmospheric reanalysis data and the synchronous composite method employed by O'Reilly and Czaja (2015) and Zhang and Luo (2017) hinder confident interpretations of the results. The disparateness of the atmospheric response to these KE indices again suggests the need for further examination.

6.3. *Impacts of OEF/SAFZ SST variability: Observations*

Table 2 summarizes current literature studies on the atmospheric response to decadal variations of the OEF or SAFZ SST. These studies have used a variety of OEF/SAFZ indices (Fig. 8c), therefore Table 2 organizes the references into groups according to the employed index, namely: (1) the latitude of maximum SST gradient, or its leading PC, (2) the mean SST, (3) the mean SST gradient, and (4) the maximum SST gradient. The indices are defined either over the SAFZ (Frankignoul et al., 2011b; Taguchi et al., 2012) or include also the KOC and KE regions (other references in Table 2), but are commonly (imprecisely) addressed as the SAFZ. Nevertheless, since the strongest SST gradient is located in the SAFZ, the inclusion of the KOC and KE regions would presumably not do too much harm. In fact, the coarse resolution of the SST data, which cannot resolve the sharp fronts very well, causes the area with the strongest SST gradient (i.e., the SAFZ) to diffuse to the whole KOE region. The definition of the SAFZ, as is obvious here, is vague. Indeed, albeit different, the indices positively correl-

Table 2. Observational studies on the OEF/SAFZ impacts on the atmosphere.

Reference	Index	Index area (°E, °N)	Time range	Dataset and resolution	Storm track response	Circulation response
Frankignoul et al. (2011b)	$lat[max(\nabla T)]_1$	*145–170, 38–45*	*1982–2008*	*OISST 0.25°, NCEP 2.5°*	—	*NPO-WP*
Yao et al. (2018)*#	$lat[max(\nabla T)]$	145–175, 35–47	1911–2010	HadISST 1°, 20CRv2 2°	↑	—
Taguchi et al. (2012)	$\overline{T}$	147.5–165.5, 37.5–42.5	1959–2006	ICOADS 2°, NCEP 2.5°	↑	–PNA
Okajima et al. (2018)*	$\overline{T}$	142–184, 35(36)–42(50)	1958–2010	ICOADS 1°, JRA55 1.25°	low-level ↑, upper-level –	–PNA
Wills and Thompson (2018)	$\overline{T}$	*140–171, 36–42*	*1979–2013*	*ERA-Interim 1.5°, ERA-Interim 1.5°*	—	*KOE low*
*Yao et al. (2019)**	$\overline{\nabla T}$	*145–175, 35–47*	*1982–2011*	*OISST 0.25°, ERA-Interim 0.75°*	*downstream +*	—
Yuan and Xiao (2018)*	$\overline{\nabla T}$	140–180, 35–45	1949–2014	HadISST 1°, NCEP 2.5°	—	+PNA
Yao et al. (2018)*#	$\max(\nabla T)$	145–170, 35–47	1911–2010	HadISST 1°, 20CRv2 2°	+	—

Note: T = SST; ∇ = gradient; $\overline{\square}$ = mean; lat = latitude; $\square_1$ = PC1; ↑ = northward shift; + = strengthening; – = weakening; — = not shown. * indicates that the study used synchronous correlation or composite analysis. # denotes that the paper did not provide a time series of the OEF/SAFZ index. Okajima et al. (2018) used a trapezoid area, and the latitude in (out of) the parentheses indicates the latitude range of the east (west) end of the trapezoid. Studies with a time range covering only 1979 and onwards are denoted with italic fonts. Resolutions before and after the comma indicate SST and atmospheric reanalysis data, respectively. The NPO-WP and PNA patterns referred to in the table are shown in Fig. 9.

ate to each other (not shown), and they all exhibit some moderate negative correlation with the Q14 KE index when the latter leads by 2–4 years, whereas the synchronous correlation is low (Fig. 8d). We note here that according to Qiu et al. (2017), the positive KE anomaly should be associated with a concurrent positive OEF-E but negative OEF-W at a delay of 2.5 years (see section 2.2), thus the delayed negative correlation and weak concurrent correlation found here is indicative of the dominance of the OEF-W over the OEF-E in terms of their connection with the KE.

The two references in group 1, respectively, presented results of the storm track and mean-flow responses and are thus hard to compare. Group 2 shows some continuity, only with Wills and Thompson (2018) as an exception. The Taguchi et al. (2012) result is supported by the same authors' high-resolution (0.5°) coupled model result, thus having added robustness. Group 3 has the same difficulty as group 1, while group 4 has only one reference. Comparing the different groups, since the indices are positively correlated, it is presumed that the groups should have consistent atmospheric impacts, yet this is not the case as shown in Table 2, with the storm track and circulation responses both showing large diversity in terms of both pattern and sign. The NPO-WP and the PNA patterns referred to in the table are shown in Fig. 9. No conclusion could be made based on these results. Taguchi et al. (2012) hypothesized that the discrepancy between their result and the results of F11 might be due to different time range and therefore different climatological background states, with their in-situ data covering 1959–2006, whereas the satellite data used in F11 cover only 1982–2008, the years after the 1977 climate shift. This is an educated guess, considering the large sensitivity to the background state revealed by a number of studies on atmospheric response to midlatitude SST anomalies (see Kushnir et al., 2002; Zhou, 2019), but more examination is needed. Another issue is still the inadequate atmospheric data resolution and the incapable analysis methods.

6.4. *Impacts of OEF/SAFZ SST variability: modeling*

There are only a few modeling studies on the issue of atmospheric impacts of OEF or SAFZ SST variability (Table 3). Taguchi et al. (2012) analyzed the output of the CFES coupled model (atmospheric resolution 110 km, oceanic resolution 0.5°) and examined the atmospheric response to an increased SAFZ SST. The model results confirmed their findings using observational data, i.e., SAFZ warming leads to a northward shift of the storm track and a negative PNA-like atmospheric response. Later, Okajima et al. (2014) took the atmospheric component of CFES, the AFES, and performed sensitivity experiments regarding the impacts of SAFZ warming in October. Their results showed that the atmospheric response is an equivalent barotropic high over the KOE, driven by a poleward-shifted storm track. Smirnov et al. (2015) forced the CAM5 AGCM with the SST anomaly regressed onto the F11 OEF index, using two different resolutions. The high-resolution (0.25°) run simulates a northward shift of the storm track, accomplished with a high over the Gulf of Alaska and a low over coastal California, which does not agree with the F11 observational results. The atmospheric response in the low-resolu-

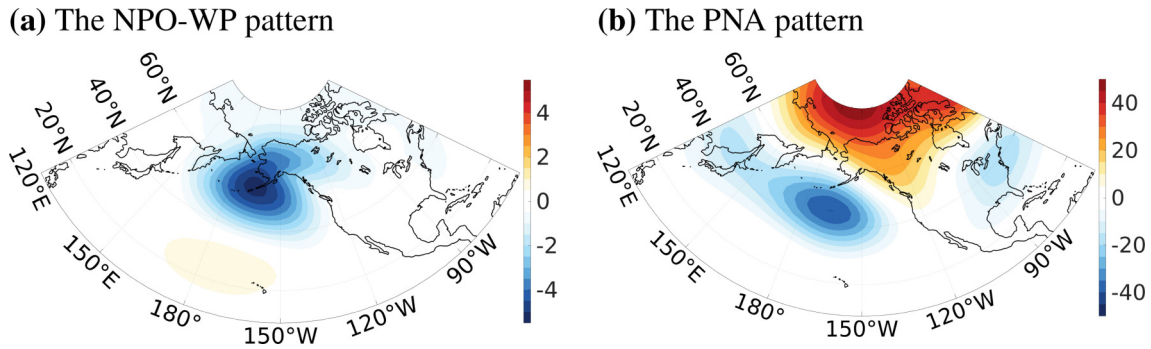

Fig. 9. (a) The positive NPO-WP pattern, defined as the 2nd empirical orthogonal function (EOF) of sea level pressure anomaly (hPa). (b) The positive PNA pattern, defined as the 1st EOF of 500 hPa geopotential height anomaly (m). Anomaly is defined as the monthly deviation from the multi-year mean annual cycle. Based on the NCEP-NCAR Reanalysis 1 dataset for 1948–2018.

Table 3. Modeling studies on OEF/SAFZ impacts on the atmosphere.

Reference	Resolution	Storm track response	Circulation response
Taguchi et al. (2012)	110 km	↑	–PNA
Okajima et al. (2014)	110 km	↑	KOE high
Smirnov et al. (2015)	0.25°	↑	Gulf of Alaska high, coastal California low
Smirnov et al. (2015)	1°	—	linear
Okajima et al. (2018)	110 km	low-level ↑, upper-level downstream –	–PNA

Note: ↑ = northward shift; – = weakening; — = not shown. The PNA pattern referred to in the table is shown in Fig. 9.

tion (1°) model, in contrast, is an equivalent barotropic linear response with low-level heating balanced by cold advection (see section 3), as a result of inadequately simulated transient eddy vorticity forcing on the mean flow. The diabatic heating profile is almost identical between the two resolutions, suggesting the important role of resolution in allowing the diabatic heating to be balanced by the right atmospheric process, either transient eddies or the mean flow. Vertical motion in the high-resolution case is much stronger, due to finer-scale structures of diabatic heating in the lower troposphere, and the anomalous mean horizontal flow in the upper levels. More recently, Okajima et al. (2018) again used the 110-km-resolution AFES to study the atmospheric response to SAFZ warming, this time focusing on January and used an artificially inflated SST anomaly. The low-level storm track, they found, shifts poleward and the upper-level storm track weakens downstream. The corresponding circulation response exhibits the negative PNA pattern, similar to, yet weaker than, the observed result of the same authors. Energy budget analysis showed that the main energy source for the circulation response is the background mean-flow available potential energy, while mean-flow and eddy kinetic energies also make remarkable contributions. The reason for the weaker-than-observed atmospheric response was attributed to insufficient conversion from eddy kinetic energy, which was further linked to a weaker background storm track, confirming that the storm track response (and thus the mean flow response) is sensitive to the storm track background state (Peng and Whitaker, 1999; Walter et al., 2001; Brayshaw et al., 2008). In contradiction with the 1°-resolution experiment of Smirnov et al. (2015) who obtained only a linear response, Okajima et al. (2018) used a similar resolution but found a significant eddy-mediated response, presumably due to the artificially inflated SST anomaly compensating the deficiency of low-resolution models in simulating latent heating induced by mesoscale precipitating systems. This argument does not agree with the finding of Smirnov et al. (2015) about nearly identical latent heating across resolutions, probably a result of the different model physics. The atmospheric circulation response to SAFZ warming or OEF northward-shift simulated in these modeling studies invariably shows a high over the North Pacific, yet the location of the high varies. However, they generally agree on the storm track response, suggesting a low-level northward shift, and a high-level downstream weakening, which is consistent with some of the observational results.

6.5. *Summary and discussion on winter results*

Based on the above discussions, it is clear that since the pioneering work of F11, observational studies on KOE frontal impacts are still insufficient and inconclusive. Probable reasons include the low data resolution, incapability of some statistical methods, and large sensitivity to the background atmospheric state, as well as the lack of knowledge about the KE and OE fronts themselves. Modeling studies focusing on the atmospheric impacts of OE decadal variability have achieved somewhat consistent results, suggesting that the storm track shifts poleward at low levels and weakens downstream at higher altitudes in response to OE strengthening and poleward migration. The role of atmospheric transient eddy feedback and the importance of model resolution are again highlighted.

Inspired by Qiu et al. (2017), here we take the view that the KE and OE are not independent, but dynamically linked. In fact, Fig. 8d evidently indicates that the OE is indeed negatively correlated with KE with a delay of 2–4 years, or positively correlated when it leads by about 2 years. The periodicity of the lead-lag correlation at ~10 years implies the decadal variability of both the KE and OE. This has some useful implications. Ideally, it is assumed that the KE and OE oscillate exactly at 10-year periods, and have a perfect correlation when KE leads by 2.5 years, as schematically illustrated in Fig. 10a (thick curves). At any time, the storm track and the atmospheric time-mean flow would "feel" the baroclinicity and latent heat forcing from both the KE and OE fronts and respond to them simultaneously. Since the KE and OE are not far from each other, passing-by transient eddies may well receive reinforcement from both and

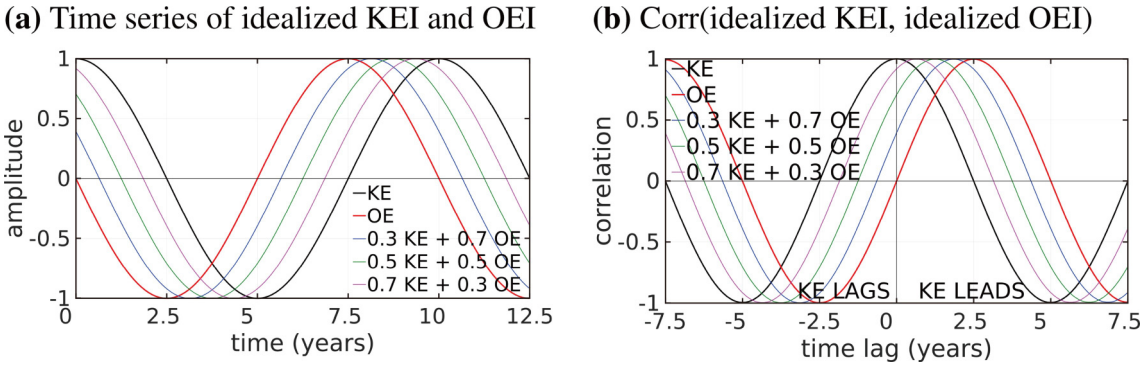

Fig. 10. (a) Time series of idealized KE and OE indices (thick curves), both having a period of 10 years, with KE leading OE by 2.5 years; and the time series of the idealized combined atmospheric impacts of the KE and OE with different linear weights (thin curves). (b) Cross-correlation between the idealized KE index (thick black curve) and the idealized OE index (thick red curve) and the combined atmospheric impacts of the KE and OE with different linear weighs (thin curves).

therefore their storm track influences could be accumulated. Further, assuming that their influences accumulate linearly and adopt different linear combination coefficients, we can obtain scenarios of the total atmospheric response from this simple linear regression model:

$$I_{AR} = \alpha I_{KE} + \beta I_{OE} + \varepsilon\,, \tag{6}$$

in which I_{AR}, I_{KE}, and I_{OE} are indices for the atmospheric response, the KE, and the OE. α and β are regression coefficients, and ε is the random error which is ignored. The time series of the total atmospheric response using different combinations of α and β are shown in Fig. 10a (thin curves), and their cross-correlation with the KE index is shown in Fig. 10b. Apparently, the more influential the OE, the closer the total response is to it. If the OE influence is significant, the synchronous atmospheric response to KE must not be the fully developed response, and using synchronous regression to find the atmospheric response to KE variability, as many studies did, would result in low or even reversed correlation. Note that here by "synchronous" we ignore the monthly-scale atmospheric response adjustment and focus on interannual to decadal timescales. Results of OE impacts suffer from the same kind of compromised synchronous correlation, yet since in reality the OEF is indeed stronger than the KEF, this effect very likely affects KE results more severely than those of the OE. Hence, examining the KE and OE atmospheric impacts separately may not be appropriate. This calls for a combined analysis of atmospheric response to KE and OE variability. The different and out-of-phase contributions from the OEF-W and OEF-E branches deserve further examination too, which certainly relies on more knowledge on the dynamics of the fronts.

6.6. *Seasonality and sensitivity to the background state*

Many studies have pointed out the seasonality of atmospheric impacts of the KOE fronts (e.g., Taguchi et al., 2009; Nakamura and Miyama, 2014; Yao et al., 2019). During boreal winter, the large heat content stored beneath the midlatitude seasonal thermocline is exposed to the sea surface by increased wind mixing (Alexander and Deser, 1995; Alexander et al., 1999), which together with the cold and dry East Asian winter monsoon blowing from Siberia, brings forth dramatic air-sea temperature contrast. Thus, the ocean releases a large amount of heat to the overlying atmosphere, marking the most intense air-sea interaction season of the year. Frontal influence on the storm track is therefore the strongest in the cold season, which is exactly the reason why many related studies, like this review, emphasize the cold season. More precisely, aside from the seasonal difference, there are even month-to-month differences within the cold season. Taguchi et al. (2012) observed a negative PNA-like atmospheric response to strengthening SAFZ in December (Table 2), but the SAFZ strengthening in January is not associated with a significant atmospheric response. Further analyses attributed the weak January response to the reduced westerly jet in response to the December SAFZ anomaly, which results in a reduction of upward air-sea fluxes that eventually hinder the frontal influence on the atmosphere in January. Modeling studies of Nakamura et al. (2004, 2008) and Sampe et al. (2010) also found the most evident front-storm track relation in mid-winter and the breakup of such a relationship in late winter. They attributed the late-winter breakup to the enhanced subtropical jet which traps the eddies inside its core and thus cannot respond to the ocean fronts. Such phenomenon, however, is not observed in the modeling results of Okajima et al. (2018). Contrary to the common belief of winter-maxima, Nakamura and Yamane (2010) found the opposite in their analysis based on the NCEP-NCAR reanalysis data and proposed a contradicting view that in winter, the baroclinicity contributed by enhanced quasi-stationary planetary waves and the large ocean-continent contrast outweighs the sensible and latent heating associated with midlatitude oceanic fronts, hence frontal influence on the storm track is even weaker than in summer. The sensitivity of the oceanic frontal impact to the atmospheric background state is thus emphasized, just like in the problem of atmospheric response to large-scale SST anomalies (Kushnir et al., 2002; Zhou, 2019). As the background state varies on monthly, seasonal, and interannual timescales, this problem can be extremely complex.

Moreover, atmospheric general circulation and storm track also undergo multi-decadal and long-term changes, especially under global warming conditions (e.g., Hare and Mantua, 2000; Yin, 2005; Iwao et al., 2012; Willison et al., 2015), which would alter the atmospheric response to frontal anomalies. As introduced above in section 6.3, this was already noticed by Taguchi et al. (2012). Révelard et al. (2016) studied the atmospheric response to KE bimodal variability for two different time periods (1979–2012 and 1959–2016) and found different results. This confirms the differential atmospheric response to frontal variability under different background states. The difference may well be related to the so-called climate regime shift around 1977, which is fundamentally a persistent phase reversal of the Pacific Decadal Oscillation (PDO; e.g., Newman et al. (2016)), yet the mechanism is yet to be fully understood. Furthermore, Qiu et al. (2014) revealed that the KE bimodal variability exhibits weaker amplitude and a shorter period before 1977, according to the OFES model (the oceanic component of CFES) hindcast, suggesting a systematic change pre and post 1977 in both the atmospheric state and the ocean. Hence, a closer investigation into the front-storm track interaction under different atmospheric and oceanic background states, particularly its future changes, is of special research interest.

7. Atmospheric impacts of mesoscale eddies and higher-frequency variability in the KOE

Besides oceanic fronts, the KOE region is also abundant in mesoscale eddies and is therefore sometimes known

as the North Pacific "oceanic storm track" (Williams et al., 2007). Mesoscale eddies in the ocean correspond to synoptic eddies in the atmosphere and hence are also known as the "ocean weather". Mesoscale eddies in the KOE are often generated from pinched-off flow loops from the meandering KE axis, having a typical spatial scale of 162 ± 28 km (mean ± standard deviation), and a lifetime of 18 ± 16 weeks (Cheng et al., 2014). The SST anomalies associated with mesoscale eddies can be up to 1.5°C, with the sub-surface temperature anomalies reaching as deep as 1000 m below the sea surface, maximizing at the core of the thermocline. Mesoscale eddies can also significantly affect the upper ocean heat content (Dong et al., 2014). Such temperature anomalies, being generated by ocean dynamics rather than forced by atmospheric variability, are potentially capable of driving atmospheric responses (Xie, 2004; Zhai and Greatbatch, 2006; Leyba et al., 2017). Although mesoscale eddies have weaker SST anomalies than oceanic fronts, their accumulated effect should nevertheless not be overlooked given their abundance. Since eddies can be regarded as fronts in curved or circular forms, their atmospheric impacts bear some similarities with those of oceanic fronts.

7.1. *MABL response to mesoscale eddies*

The SST and upper ocean heat content anomaly associated with mesoscale eddies force changes of the overlying atmospheric state via anomalous sensible and latent heating. Warm eddies, for example, cause the near-surface air temperature to increase and air pressure to decrease, which then trigger secondary circulation with low-level convergence and updraft (Lindzen and Nigam, 1987). The increased air temperature reduces atmospheric static stability and enhances vertical turbulent mixing (Wallace et al., 1989). In the meantime, more vapor is evaporated and transported aloft by the updraft and mixing, therefore increasing cloud cover, precipitation, and latent heating (Bourras et al., 2004; Chelton et al., 2004, 2011; O'Neill, 2012; Frenger et al., 2013; Lambaerts et al., 2013; Bôas et al., 2015; Renault et al., 2016; Putrasahan et al., 2017; Sugimoto et al., 2017). The downward momentum transport by turbulent mixing and the low-level convergence associated with the pressure adjustment both increase near-surface wind, leading to a positive correlation between SST and wind anomalies (Liu et al., 2000; Chelton et al., 2001; Hashizume et al., 2001; Nonaka and Xie, 2003; Skyllingstad et al., 2007; O'Neill et al., 2010; Chelton, 2013; Rouault et al., 2016; Ma et al., 2017; Sugimoto et al., 2017; Gao et al., 2019). The positive SST-wind correlation contradicts the conventional belief that the atmosphere forces the ocean (strong wind brings cold and dry air that cools the ocean) and was what evoked interest in mesoscale air-sea interaction studies in the first place. The two mechanisms, i.e., the vertical mixing mechanism and the pressure adjustment mechanism, are active in different circumstances: the former is believed to be relatively rapid and thus more responsible for small spatial and temporal scales (e.g., transient ocean eddies and cross-frontal wind), whereas the pressure adjustment mechanism needs more time and is more suitable for persistent oceanic anomalies (e.g., quasi-stationary eddies and along-frontal wind). Recently, Chen et al. (2017) performed composite analysis on oceanic and atmospheric mesoscale anomalies in the KOE region and found that in this region, about 60% of the mesoscale eddies impact the atmosphere via the vertical mixing mechanism, and 10% via the pressure adjustment mechanism, while the other 30% are too weak to exert any influence on the atmosphere. Such effects are sometimes confined within the MABL (Bourras et al., 2004; Frenger et al., 2013; Perlin et al., 2014), but can sometimes penetrate through the boundary layer to the free atmosphere (Ma et al., 2015a, 2016; Sugimoto et al., 2017; Chen et al., 2017). The readers are referred to Small et al. (2008) for a thorough (albeit perhaps outdated) review on MABL response to mesoscale eddies.

7.2. *Storm track and free-atmospheric response to mesoscale SST anomalies*

Influences of single mesoscale eddies on the boundary layer atmosphere have been under active research for years, but it is only up until recent years that their accumulated impacts on the storm track started drawing attention. Previous studies (e.g., Frenger et al., 2013; Chen et al., 2017) commonly examined the atmospheric impacts of mesoscale eddies in the sense of composite-mean, i.e., the mean over a large number of eddies. As such, those results represent the atmospheric signature of a typical warm or cold eddy with moderate strength and circular-shaped SST anomalies corresponding well with the SSH anomalies. However, when passing by the ocean surface, extratropical cyclones encounter many eddies, both warm and cold, with various strengths and differently distorted shapes. How would the cyclones be affected by those eddies accumulatively, especially whether the effects of warm and cold eddies cancel out, is an interesting question.

Two points must be noted here, though. First, mesoscale eddies are often detected based on their SSH signatures, e.g., by means of closed SSH contours (Faghmous et al., 2015), yet their atmospheric influences are most commonly studied as a response to their SST anomalies. Individual eddies often have non-matching SSH and SST anomalies. There are also SST-based eddy detection methods (Dong et al., 2011; Zhang et al., 2015), but they do not necessarily give identical results as SSH-based methods. Particularly, an eddy with a closed SSH contour may not have a closed SST contour and therefore not be identified as one by SST-based methods. This discrepancy reflects the dynamic and thermodynamic perspectives of the ocean mesoscale, and is also suggestive of the difference between the eddy-induced temperature anomalies at the surface and those over the whole water column since the eddy SSH anomaly is linearly related to heat content anomaly due to the thermal expansion effect (e.g., Stephenson et al., 2013). Therefore, it should be considered that the mesoscale eddies referred to in the context of this section might not be the same as those examined by studies of eddy dynamics.

Second, for convenience, spatial filtering is often used to extract the mesoscale SST features instead of SST-based eddy identification. Typical filters include the simplest boxcar filter, and the more sophisticated Loess filter, operating on, e.g., 5° × 5° windows to extract the larger scale, which is then subtracted from the original to get the smaller scale, the mesoscale. Since oceanic fronts and eddies are both mesoscale features, this method is not efficient in separating the two (Zhang et al., 2019a). As a result, fronts likely coexist with eddies in the filtered SST field. As such, at least part of the atmospheric impacts of this kind of mesoscale SST comes from fronts but is sometimes misinterpreted as from eddies. To alleviate this problem, elongating the filtering window in the zonal direction, say, to 15° × 5° (longitude × latitude), could yield some improvement, but cleaner separation could be achieved by using a good SST-based eddy detection algorithm. Base on the above two points, the SST features thus obtained is more strictly referred to using the term "mesoscale SST anomalies", instead of "mesoscale eddies", but it should be noted that sometimes this distinction is not explicitly made.

Using a high-resolution (27 km) regional model, Ma et al. (2015b) found that the intensity of the North Pacific storm track would decrease by 15% if the KOE mesoscale SST anomalies are removed. Diagnostics show that the ensemble of eddies accumulates diabatic heating, of which latent heating is the main component, and thereby forces the atmospheric eddies by conversion to eddy kinetic energy. The reason why the positive and negative latent heating anomalies associated with warm and cold eddies do not exactly cancel out is attributed to the nonlinearity of the Clapeyron-Clausius relation, an empirical but accurate approximation of which is given by Bolton (1980):

$$e_s = 6.112\exp\left(\frac{17.67T}{T+243.5}\right), \tag{7}$$

where e_s is the saturation vapor pressure in hPa, and T is temperature in °C. By the same absolute value of temperature anomaly, saturation vapor pressure is increased more over warm eddies than it is decreased over cold eddies. For example, for the standard atmosphere (background sea surface air temperature = 15°C = SST), a +1°C warming would increase e_s by 6.62%, yet a −1°C cooling reduces it by 6.26%. Hence, the overall vapor amount is increased over a sea surface with fluctuating temperature, even if the mean over the temperature fluctuation is zero. Ma et al. (2017) further confirmed that such phenomenon is highly dependent on the model resolution, as a low-resolution (162 km) regional model failed to simulate the mesoscale eddy forcing on the storm track. More recently, Zhang et al. (2019b) further investigated the influence of mesoscale SST in the KOE region on the storm track by detecting and tracking the extratropical cyclones in the experiments of Ma et al. (2015b). Thereby they found that the presence of mesoscale SST anomalies almost doubles water vapor supply, and the resultant increase of diabatic heating supports cyclone intensification.

However, using a high-resolution (0.23°) coupled atmosphere-slab ocean model, Jia et al. (2019) recently showed that although ocean mesoscale eddies drive significant enhancement of storm track and vertical moisture fluxes and hence total precipitable water, no precipitation changes are found. Other modeling research on the atmospheric influence of mesoscale eddies includes the idealized regional modeling of Foussard et al. (2019). They artificially added mesoscale SST perturbations in a straight frontal zone and found that the westerly jet and the storm track both shift northward due to the added mesoscale SST signals. Sun et al. (2018), moreover, employed a low-resolution (2° longitude × 2.5° latitude) AGCM, but prescribed stochastic SST disturbances at each grid point that are different from month to month in the KOE, and found significant storm track enhancement, with energy sources from both increased low-level baroclinicity and latent heating. Their grid-point monthly SST noise does not exactly represent mesoscale eddies, but it does have the same spatial scale as relatively large mesoscale eddies in the KOE (Cheng et al., 2014), while its month-to-month evolution is analogous to timescales of short-lived eddies. The magnitude of the stochastic SST anomaly (standard deviation = 0.5°C) is similar to that of SST anomalies associated with relatively weak KOE eddies (Chen et al., 2017). Therefore, their results are in a way suggestive of the potential roles of mesoscale eddies on the storm track. Zhang et al. (2020b) recently repeated the experiments of Ma et al. (2015b) with an AGCM, and found that after removing the KOE mesoscale SST structures, the low-level storm track decreases by about 20% along the KOE and shifts southward downstream alongside a precipitation reduction of 7%. Also in line with these findings, the recent modeling work of Liu et al. (2021) reveals that the reinforcement of extratropical cyclones by the KOE mesoscale SST-induced excessive moisture supply leads to enhanced moisture transport away from the cyclone by airflow in the warm sector. This additional moisture source feeds into the atmospheric river (WS-NE-oriented plumes of intense vapor transport from above the ocean to the western coast of North America) and is responsible for the increase of heavy precipitation when the atmospheric river makes landfall.

7.3. *Storm track and free-atmospheric response to higher-frequency SST variability*

Focusing on even higher-frequency SST variability than the mesoscale, Zhou et al. (2015) used a high-resolution (0.56°) global AGCM and highlighted the role of high-frequency (1–10 days) KOE SST fluctuations in changing atmospheric stability and thus baroclinicity, thereby favoring energy conversion from the time-mean flow to transient atmospheric eddies in the storm track. Their results suggested a greater role of anomalous stability than horizontal temperature gradient (or vertical wind shear) for baroclinicity. High-frequency SST variability on timescales shorter than 10 days, which has long been regarded as "noise" and ignored in climate models, might have to be considered. In

interpreting this result, it is useful to note that the 1–10 day variability corresponds roughly to the better-known submesoscale processes, which are on the temporal scale of O (1/24–10) days (e.g., Thomas et al., 2008; Qiu et al., 2016, 2020a; McWilliams, 2016). Considering that the SST forcing data has a temporal resolution of one day, submesoscale processes can be partially resolved in the time domain. However, the AGCM's spatial resolution is too crude for the submesoscale, whose spatial scale is O (0.1–200) km. Therefore, the high-frequency SST fluctuations highlighted in Zhou et al. (2015, 2017) are merely some residual of unresolved submesoscale processes. Nevertheless, the proposed importance of such oceanic high-frequency variability on the storm track likely suggests an even bigger role of the full submesoscale processes. Likely related to this, Tian et al. (2017) used a coupled climate model with an atmospheric resolution of 1.87° and oceanic resolution of 1.5° and showed great sensitivity of air-sea fluxes when the coupling frequency is increased from once per day to once per hour. This is thus indicative of the significant air-sea interaction involving oceanic high-frequency processes.

These recent studies start to reveal the potential influences of mesoscale and even higher-frequency (partially submesoscale) SST perturbations on the atmospheric storm track, pushing the frontier of our understanding of air-sea interaction to even smaller scales. The characteristics and mechanism of such influences are yet to be more thoroughly explored. More high-resolution modeling studies are needed to confirm the findings and evaluate the model dependency. Observational confirmation is also highly needed, which would not be possible without high-resolution oceanic and atmospheric observational or reanalysis data for the same reason as for studies on frontal impacts. However, submesoscale-resolving long-term model simulations are expensive, and observational studies are subject to the added difficulty of separating impacts from fronts, eddies, and even submesoscale processes, which are most likely present at the same time.

7.4. *Possible decadal modulation by mesoscale and higher-frequency variability*

As introduced in section 2, mesoscale eddy activity is an integral part of the KOE dynamical system. There has been extensive observational evidence that confirmed the decadal variability of eddy activity in the KOE, either in terms of eddy kinetic energy (Qiu and Chen, 2005; e.g., Taguchi et al., 2007; Ding et al., 2018) or SST standard deviation (Sugimoto and Hanawa, 2011; Seo et al., 2014; Zhou et al., 2017). Given the newly proposed argument that mesoscale eddies have significant accumulated effects on the storm track, the interannual-decadal variability of eddy activity is most likely also capable of modulating the storm track and atmospheric general circulation. It must be noted, though, that just as KE and OE impacts should be preferably considered in one framework (section 6.5), impacts of decadal variability of eddy activity, if there is indeed any, most probably do not work alone either. Furthermore, recent findings proposed that high-frequency SST variability (oceanic "noise level") could also play a significant role. As ocean high-frequency variability roughly corresponds, in a sense, to submesoscale processes, and submesoscale processes are dynamically linked to the mesoscale via mixed-layer instability and strain-induced frontogenesis (Thomas et al., 2008; McWilliams, 2016), therefore, decadal-scale atmospheric modulation by the dynamically integrated multi-scale KOE system is of high research interest.

Direct investigations into this perspective are still scarce. Based on high-resolution AGCM experiments, Zhou et al. (2017) proposed that the relative strength of KOE fronts and ocean high-frequency variability has the potential to modulate the North Pacific storm track and atmospheric circulation on decadal timescales. Particularly, during the 20 years spanning 1980–99, the OE fronts have a linearly increasing trend, while at the same time the level of high-frequency variability is decreasing. Meanwhile, the atmospheric response in the North Pacific sector to the same SST anomaly gradually switches from a trough to a ridge. Given the importance of fronts and high-frequency variability discussed above, the authors thus speculated that the higher level of high-frequency variability in the former decade drives an eddy-mediated response, while in the latter decade the stronger OE fronts are in control. This, however, needs further confirmation by other modeling studies and by observation. On the other hand, Zhang et al. (2019a) defined a mesoscale SST anomaly index based on 0.25° NOAA OISST and studied atmospheric anomalies associated with the positive and negative phases of this index using 2.5° NCEP/NCAR reanalysis for the period 1985–2005. It was found that the storm track is shifted southwards during the positive phase of the index, which is driven by turbulent heat flux changes and hence anomalous baroclinicity. Their results, however, are subject to the same difficulties as those of the observational studies on roles of the oceanic fronts (section 6.1), since low-resolution atmospheric fields and synchronous composite analysis are used. Furthermore, the mesoscale SST index was defined as the area and monthly average of daily variance of mesoscale features extracted by a 5° × 5° boxcar filter, which, as discussed in section 7.2, cannot quite distinguish SST fronts and mesoscale eddy-induced SST perturbations. In fact, the aforementioned index exhibits a good correlation with the SAFZ frontal index defined by Yao et al. (2018; see Table 2). The above results, therefore, should not be simply interpreted as representing interannual-decadal modulation of mesoscale eddy variability, as they might also include the roles of frontal variability. Future studies should focus upon additional high-resolution modeling efforts and observational datasets, with carefully designed methods to extract eddy-induced SST anomalies and, thereby, new definitions of its index.

8. North Pacific climate variability mediated by KOE fronts

The decadal variations of the KOE fronts have import-

ant implications for climate variability in the North Pacific sector. On one hand, decadal KE variability is at least partially driven by basin-scale wind stress variability (section 2.3); and on the other hand, decadal KE variability and the associated SAFZ variability, can modulate atmospheric storm track and circulation changes (section 6) which can feedback to the KE system by generating new SSH anomalies. A closed climate feedback loop is thus probable (Liu and Di Lorenzo, 2018). This feedback loop is different from the one proposed by Latif and Barnett (1994) based on climate model simulations. In the latter, the oceanic mechanism is the wind-driven intensification of the subtropical gyre and hence the enhanced heat transport by the Kuroshio and the KE, which further drive large-scale atmosphere wind anomalies mediated by transient eddies (section 3), that closes the loop. The timescale of this coupled feedback is estimated to be as long as a few decades. As introduced above, however, the basin-scale wind anomalies also force westward-propagating Rossby waves which arrive at the KOE region and bring about oceanic frontal changes in just a few years. The KOE fronts, therefore, are the bridge of a faster feedback mechanism that enhances the KOE ocean spectrum in the decadal band.

To explore the KOE front-mediated climate feedback mechanism, Qiu et al. (2007) put forth a coupled prediction model of SST in the KE band (32°–38°N, 142°–180°E) based on observational and reanalysis data for 1948–2005. In this model, the KE SST is controlled by red-spectral thermal damping and white-spectral atmospheric forcing, as in the conventional stochastic climate model (Hasselmann, 1976; Frankignoul and Hasselmann, 1977), as well as from the contribution from local SSH signals which physically represents the warm water advection by the KE jet. The SSH signal is further determined by the Rossby wave propagation from the central North Pacific driven by basin-scale wind stress curl anomalies:

$$\begin{cases} \dfrac{\partial T}{\partial t} = ah - \lambda T + q \\ \dfrac{\partial h}{\partial t} - C_{\mathrm{R}} \dfrac{\partial h}{\partial x} = -\dfrac{g' \mathrm{curl}\boldsymbol{\tau}}{\rho_0 g f} \end{cases}, \tag{8}$$

where T is SST, h is SSH, a is a coefficient for SSH contribution to SST determined empirically, λ is the damping factor estimated from the decorrelation time scale of SST, q is white noise forcing whose standard deviation is obtained empirically, C_{R} is the Rossby wave propagation speed at the KE latitudes estimated from satellite measurements after 1992, g' is reduced gravity, ρ_0 is a reference density, f is the Coriolis parameter, and $\boldsymbol{\tau}$ is the wind stress anomaly.

To account for the coupled feedback of the wind stress curl from the KE variability, the wind stress curl term is decomposed into an intrinsic part taken as the leading two EOF modes of observed wind stress curl variability, and an SST-feedback part represented by the KE SST multiplied by a coupling coefficient estimated from the linear regression between the SST and the wind stress curl when SST leads by three months to account for the atmospheric adjustment time. It was shown that the model does a better job in representing the decadal variability of KE SST than the uncoupled case where the wind stress curl anomaly is only expressed by the intrinsic part. Similar to this approach, Qiu et al. (2014) developed a coupled prediction model for the KE index defined as the box-averaged SSH over the KE region (31°–36°N, 140°–165°E) based on the merged results of satellite observations and the OFES model after 1977. The difference with their previous work is that the predictand is now SSH, and the wind stress curl anomaly has only the feedback part, the coupling coefficient of which is still estimated empirically with an atmospheric adjustment time of two months. This model was shown to have a better skill in hindcasting the KE index than in the uncoupled case, especially at lead times of four years and above, when the wind stress curl anomaly switches sign.

The above studies improved the prediction of North Pacific decadal climate variability by considering the atmospheric response to anomalies of the ocean western boundary current and frontal systems. However, the current understanding is still very much limited. In fact, the coupled empirical KE SST and SSH predictions of Qiu et al. (2007, 2014) only account for a small percentage of the observed SST and SSH variability (9.3% of monthly SST and 27.4% of decadal and longer SST, 45% of SSH variability at a 3-year prediction lead time and 30% at a 4-year lead time). This reflects the complexity of the coupled problem. First of all, from the pure oceanic point of view, the dynamics of the KOE system, including the interaction between the jets, fronts, and eddies, has not yet been fully understood (sections 2.1 and 2.2). Second, the response of the KOE to wind forcing, especially the relative roles of wind forcing and intrinsic oceanic processes, is still debatable (section 2.3). Third, and related to the above two points, the atmospheric response to changes of the KOE oceanic processes is still poorly known. Ignorance of the OE fronts and/or mesoscale eddies could be a possible reason, given their importance in modulating the storm track too (section 6). Moreover, we note that the climate regime shift around 1977, which is associated with dramatic changes of both the atmosphere and ocean, may also hinder the prediction skill. Qiu et al. (2007), for example, estimated the Rossby wave propagation speed and SSH contribution to SST purely based on post-1977 data but used them for the whole period back to 1948. Clearly, there still exists large uncertainty over the KOE-mediated decadal climate feedback regarding each of its components: the ocean, the atmosphere, and their two-way interactions. Much more work is needed before a better picture of North Pacific decadal climate feedback mediated by KOE fronts and eddies is possible.

9. Summary and concluding remarks

In this paper, we have reviewed the current research progress regarding atmospheric impacts of midlatitude oceanic

fronts and eddies. The atmospheric impacts consist of two major parts—the impacts on the time-mean flow and the impacts on synoptic transient eddies, the latter of which also comprises two aspects, i.e., single eddies (storms) and their statistics—the storm track. Some of the discussions concerned the atmospheric impacts of oceanic fronts in general, but the emphasis was made on fronts in the KOE region, especially regarding their decadal modulation of the atmosphere. As in many literature studies, we focused on the winter season, when air-sea interaction is the most intense, completed with a brief discussion on seasonal contrast. Potential differences of the atmospheric impacts of the KOE fronts under different climatological atmospheric and oceanic background states are also discussed, as well as the climate feedback mechanism based on observations made in recent decades. Finally, the emerging acknowledgment of the importance of mesoscale eddies and higher frequency oceanic variability to the storm track and atmospheric circulation, as revealed by recent modeling studies, is introduced.

The current understanding and remaining issues can be summarized as follows:

- MABL models based on the Ekman balance and mixed layer assumption have been proposed to explain the frontal impacts on the atmospheric time-mean flow in the case of along-frontal wind. Free-atmospheric impacts of the fronts can also be inferred. These models adopt the hydrostatic pressure adjustment to the SST gradient and predict a band of convergence and updraft anchored to the warm flank of the oceanic front. For a cross-frontal wind, the mixed layer assumption breaks up, and the pressure adjustment mechanism is replaced by differential vertical turbulent mixing associated with the cross-frontal SST contrast. The vertical mixing mechanism generally needs less adjustment time and is thus favorable for cross-frontal winds and mesoscale eddies.
- A band of increased high cloud and enhanced precipitation in the time-mean to the south of the front was noticed in the observations and was originally regarded as evidence to the free-atmospheric mean-flow response predicted by the MABL models that lack moist processes. Recently, however, doubt has been cast upon the validity of this interpretation. Some studies showed that the time-mean convergence and precipitation could be a residual imprint of the transient eddy response, as a result of the skewness of the eddy-associated convergence, updraft, and precipitation anomalies. It is thus a challenge for observational studies to properly isolate the presumably weak time-mean response from the more dominant transient eddy response, in order to ensure a fair comparison with the theoretical results.
- The response of the individual transient eddies, i.e., the extratropical cyclones and anticyclones, involves interactions between the SST front and different mesoscale components of the cyclone, including the atmospheric front (mainly the cold front), convection in the cold sector, and the warm conveyor belt. It has been argued that the SST front is responsible for an increased frequency of atmospheric frontal occurrence, enhanced precipitation in the cold sector, and a reinforced updraft in the warm conveyor belt. However, related studies are still scarce and more detail on the dynamical and thermodynamical ocean-atmospheric mesoscale linkage is clearly needed.
- The SST frontal impact on the storm track, i.e., the statistics of extratropical cyclones and anticyclones, has been confirmed by numerous modeling studies. The storm track position and strength are modulated by the frontal position and strength by means of the following three factors: the strong sensible forcing on cross-frontal air temperature gradient which contributes to low-level baroclinicity, the differential atmospheric stability across the front contributing also to low-level baroclinicity, and the huge latent heating aloft over the warm flank which works to enhance mid-level baroclinicity. There still lacks a consensus regarding the relative roles of these factors, which are related to the relative importance of the SST gradient and its absolute value.
- The KOE currents and fronts exhibit decadal-scale fluctuations largely controlled by the bimodal variability of the KE. Some studies have attempted to use observational measures to evaluate the influence of such decadal variability on the atmosphere. However, these studies, focusing on atmospheric responses to either the KE or the OE frontal variability, have come to disparate conclusions. Possible reasons for the uncertainties include: the inadequate resolution of the reanalysis data, the incapability of some of the statistical methods in distinguishing response from forcing, the sensitivity to the artificially chosen atmospheric adjustment time to SST forcing, the different external-forcing removal treatment, the lack of knowledge on the fronts themselves which hinders the choice of a good index for frontal variability, the ignorance of the combined and delayed response to both the KE and OE frontal variabilities, and the sensitivity of the response to the climatological background state.
- Modeling studies, albeit rare, were able to reach a more consistent response of the storm track to decadal meridional migration of the OE, indicating a northward shift of the low-level storm track and a downstream weakening of the upper-level storm track in response to a northward OE shift. No attempts were made to consider the influences of KE variability either separately or combined with the OE.
- Large sensitivity to the background state is found based on both observational and modeling studies. Sea-

sonal, interannual, and multi-decadal changes of the background state can all alter the atmospheric response to KOE fronts. This reflects the eddy-mediated nature of the response since the storm track background state certainly determines how it would respond to changes at the lower boundary, as has been learned from the extensive studies on atmospheric response to large-scale midlatitude SST anomalies.

- Based on the extensive research on MABL impacts of mesoscale eddies, a few recent modeling studies highlighted the role of the KOE mesoscale eddies to the storm track. It has been shown that the accumulated effects of the mesoscale eddies can increase low-level baroclinity and mid-level latent heating, and thereby favor atmospheric transient eddy development. The importance of even higher-frequency ocean perturbations partially corresponding to submesoscale processes is also proposed by recent modeling studies. However, related studies are scarce, and observational confirmation is still lacking.
- The decadal modulation of the KOE fronts on the atmosphere has the potential to form a closed decadal climate feedback of the North Pacific sector since the decadal variation of the KE itself is presumably triggered by fluctuations of wind-induced SSH anomalies. Coupled empirical feedback theories have been proposed and they do have some skill in predicting the North Pacific decadal climate variability. However, the current models can only explain a small fraction of the total SSH and SST variability of the KOE, probably due to the limited knowledge on both ways of the mutual air-sea interaction, as well as the sensitivity to the background state.

A better understanding of the atmospheric impacts and the potential climate feedback is only possible through the advancement of oceanographic research on dynamics of the integrated KOE system, including the KE jet, branches of the OE jet, the KE and OE fronts, and the mesoscale eddies and submesoscale processes. On the other hand, the advancement of meteorological studies on extratropical cyclone mesoscale dynamics involving fronts and convection is also necessary. It is thus key to future studies to better resolve the interaction between oceanic and atmospheric mesoscale and submesoscale processes, as well as the interaction between these finer-scale processes with the larger scale oceanic and atmospheric circulation. However, in order to achieve more confident results, high-resolution observational or reanalysis data and numeric models accurately representing oceanic fronts and mesoscale eddies, and preferably even the submesoscale processes, must be employed. Among others, the recently published ERA5 long-term reanalysis dataset developed by the ECMWF with a resolution of 30 km (Hersbach et al., 2020) could be a good start. Although, in a strict sense, its resolution is still only eddy-permitting for the ocean and not convection-permitting for the atmosphere, it is indeed expected to greatly improve the representation of the ocean mesoscales' imprint on the atmosphere than traditional datasets. In recent years, global oceanic submesoscale-permitting and atmospheric convection-resolving simulations [both having grid spacing of $O(1)$ km] have emerged (e.g., Rocha et al., 2016; Stevens et al., 2019), yet these simulations are limited to short time periods. Moreover, the value of coupled atmosphere-ocean modeling in studying mesoscale and even submesoscale air-sea interaction must be emphasized. Recent findings revealed that the atmospheric imprints of mesoscale eddies can feedback to the ocean by both thermally and mechanically damping the eddies (Ma et al., 2016; Renault et al., 2019). Enabling coupling could thus result in weaker eddy activity, and hence weaker eddy-mean flow interaction, eventually fixing a long-standing modeling bias: the underestimate of western boundary currents. The weaker eddies and stronger currents could possibly further feedback on the atmosphere and alter the mesoscale and frontal scale air-sea interaction. Finally, care must be taken as the atmospheric response depends on the background state of the atmosphere and the ocean; therefore, it may change in climatological terms. Long-term data coverage and coupled atmosphere-ocean model integration are thus useful.

Acknowledgements. This work is supported by the National Natural Science Foundation of China (Grant No. 41906001), the Natural Science Foundation of Jiangsu Province (Grant No. BK20190501), and the Fundamental Research Funds for the Central Universities (Grant No. B210202137).

REFERENCES

Alexander, M. A., and C. Deser, 1995: A mechanism for the recurrence of wintertime midlatitude SST anomalies. *J. Phys. Oceanogr.*, **25**, 122–137, https://doi.org/10.1175/1520-0485(1995)025<0122:AMFTRO>2.0.CO;2.

Alexander, M. A., C. Deser, and M. S. Timlin, 1999: The reemergence of SST anomalies in the North Pacific Ocean. *J. Climate*, **12**, 2419–2433, https://doi.org/10.1175/1520-0442(1999)012<2419:TROSAI>2.0.CO;2.

Belkin, I., R. Krishfield, and S. Honjo, 2002: Decadal variability of the North Pacific Polar Front: Subsurface warming versus surface cooling. *Geophys. Res. Lett.*, **29**, 65-1–65-4, https://doi.org/10.1029/2001GL013806.

Bjerknes, J., and H. Solberg, 1922: Life cycle of cyclones and the polar front theory of atmospheric circulation. *Geofys. Publ.*, **3**, 3–18.

Bôas, A. B. V., O. T. Sato, A. Chaigneau, and G. P. Castelão, 2015: The signature of mesoscale eddies on the air-sea turbulent heat fluxes in the South Atlantic Ocean. *Geophys. Res. Lett.*, **42**, 1856–1862, https://doi.org/10.1002/2015GL063105.

Bolton, D., 1980: The computation of equivalent potential temperature. *Mon. Wea. Rev.*, **108**, 1046–1053, https://doi.org/10.1175/1520-0493(1980)108<1046:TCOEPT>2.0.CO;2.

Booth, J. F., L. A. Thompson, J. Patoux, K. A. Kelly, and S. Dickinson, 2010: The signature of the midlatitude tropospheric

storm tracks in the surface winds. *J. Climate*, **23**, 1160–1174, https://doi.org/10.1175/2009JCLI3064.1.

Booth, J. F., L. Thompson, J. Patoux, and K. A. Kelly, 2012: Sensitivity of midlatitude storm intensification to perturbations in the sea surface temperature near the Gulf Stream. *Mon. Wea. Rev.*, **140**, 1241–1256, https://doi.org/10.1175/MWR-D-11-00195.1.

Bourras, D., G. Reverdin, H. Giordani, and G. Caniaux, 2004: Response of the atmospheric boundary layer to a mesoscale oceanic eddy in the northeast Atlantic. *J. Geophys. Res.: Atmos.*, **109**, D18114, https://doi.org/10.1029/2004JD004799.

Brachet, S., F. Codron, Y. Feliks, M. Ghil, H. Le Treut, and E. Simonnet, 2012: Atmospheric circulations induced by a midlatitude SST front: A GCM study. *J. Climate*, **25**, 1847–1853, https://doi.org/10.1175/JCLI-D-11-00329.1.

Branstator, G., 2002: Circumglobal teleconnections, the jet stream waveguide, and the North Atlantic Oscillation. *J. Climate*, **15**, 1893–1910, https://doi.org/10.1175/1520-0442(2002)015<1893:CTTJSW>2.0.CO;2.

Brayshaw, D. J., B. Hoskins, and M. Blackburn, 2008: The storm-track response to idealized SST perturbations in an aquaplanet GCM. *J. Atmos. Sci.*, **65**, 2842–2860, https://doi.org/10.1175/2008JAS2657.1.

Brayshaw, D. J., B. Hoskins, and M. Blackburn, 2009: The basic ingredients of the North Atlantic storm track. Part I: Land-sea contrast and orography. *J. Atmos. Sci.*, **66**, 2539–2558, https://doi.org/10.1175/2009JAS3078.1.

Brayshaw, D. J., B. Hoskins, and M. Blackburn, 2011: The basic ingredients of the North Atlantic storm track. Part II: Sea surface temperatures. *J. Atmos. Sci.*, **68**, 1784–1805, https://doi.org/10.1175/2011JAS3674.1.

Broccoli, A. J., and S. Manabe, 1992: The effects of orography on midlatitude northern hemisphere dry climates. *J. Climate*, **5**, 1181–1201, https://doi.org/10.1175/1520-0442(1992)005<1181:TEOOOM>2.0.CO;2.

Bryan, F. O., R. Tomas, J. M. Dennis, D. B. Chelton, N. G. Loeb, and J. L. McClean, 2010: Frontal scale air-sea interaction in high-resolution coupled climate models. *J. Climate*, **23**, 6277–6291, https://doi.org/10.1175/2010JCLI3665.1.

Businger, S., T. M. Graziano, M. L. Kaplan, and R. A. Rozumalski, 2005: Cold-air cyclogenesis along the Gulf-Stream front: Investigation of diabatic impacts on cyclone development, frontal structure, and track. *Meteor. Atmos. Phys.*, **88**, 65–90, https://doi.org/10.1007/s00703-003-0050-y.

Catto, J. L., C. Jakob, G. Berry, and N. Nicholls, 2012: Relating global precipitation to atmospheric fronts. *Geophys. Res. Lett.*, **39**, 1–6, https://doi.org/10.1029/2012GL051736.

Ceballos, L. I., E. Di Lorenzo, C. D. Hoyos, N. Schneider, and B. Taguchi, 2009: North Pacific gyre oscillation synchronizes climate fluctuations in the eastern and western boundary systems. *J. Climate*, **22**, 5163–5174, https://doi.org/10.1175/2009JCLI2848.1.

Chang, E. K. M., and I. Orlanski, 1993: On the dynamics of a storm track. *J. Atmos. Sci.*, **50**, 999–1015, https://doi.org/10.1175/1520-0469(1993)050<0999:OTDOAS>2.0.CO;2.

Chang, E. K. M., S. Lee, and K. L. Swanson, 2002: Storm track dynamics. *J. Climate*, **15**, 2163–2183, https://doi.org/10.1175/1520-0442(2002)015<02163:STD>2.0.CO;2.

Charney, J. G., 1947: The dynamics of long waves in a baroclinic westerly current. *J. Atmos. Sci.*, **4**, 136–162, https://doi.org/10.1175/1520-0469(1947)004<0136:TDOLWI>2.0.CO;2.

Chelton, D., 2013: Mesoscale eddy effects. *Nature Geoscience*, **6**, 594–595, https://doi.org/10.1038/ngeo1906.

Chelton, D. B., M. G. Schlax, M. H. Freilich, and R. F. Milliff, 2004: Satellite measurements reveal persistent small-scale features in ocean winds. *Science*, **303**, 978–983, https://doi.org/10.1126/science.1091901.

Chelton, D. B., and Coauthors, 2001: Observations of coupling between surface wind stress and sea surface temperature in the eastern tropical Pacific. *J. Climate*, **14**, 1479–1498, https://doi.org/10.1175/1520-0442(2001)014<1479:OOCBSW>2.0.CO;2.

Chelton, D. B., M. G. Schlax, and R. M. Samelson, 2011: Global observations of nonlinear mesoscale eddies. *Progress in Oceanography*, **91**, 167–216, https://doi.org/10.1016/j.pocean.2011.01.002.

Chen, L. J., Y. L. Jia, and Q. Y. Liu, 2017: Oceanic eddy-driven atmospheric secondary circulation in the winter Kuroshio Extension region. *Journal of Oceanography*, **73**, 295–307, https://doi.org/10.1007/s10872-016-0403-z.

Chen, S. M., 2008: The Kuroshio Extension Front from satellite sea surface temperature measurements. *Journal of Oceanography*, **64**, 891–897, https://doi.org/10.1007/s10872-008-0073-6.

Cheng, Y. H., C. R. Ho, Q. A. Zheng, and N. J. Kuo, 2014: Statistical characteristics of mesoscale eddies in the North Pacific derived from satellite altimetry. *Remote Sensing*, **6**, 5164–5183, https://doi.org/10.3390/rs6065164.

Davis, R. E., 1976: Predictability of sea surface temperature and sea level pressure anomalies over the North Pacific Ocean. *J. Phys. Oceanogr.*, **6**, 249–266, https://doi.org/10.1175/1520-0485(1976)006<0249:POSSTA>2.0.CO;2.

Davis, R. E., 1978: Predictability of sea level pressure anomalies over the North Pacific Ocean. *J. Phys. Oceanogr.*, **8**, 233–246, https://doi.org/10.1175/1520-0485(1978)008<0233:POSLPA>2.0.CO;2.

De Vries, H., S. Scher, R. Haarsma, S. Drijfhout, and A. V. Delden, 2019: How Gulf-Stream SST-fronts influence Atlantic winter storms. *Climate Dyn.*, **52**, 5899–5909, https://doi.org/10.1007/s00382-018-4486-7.

Dee, D. P., and Coauthors, 2011: The ERA-Interim reanalysis: Configuration and performance of the data assimilation system. *Quart. J. Roy. Meteor. Soc.*, **137**, 553–597, https://doi.org/10.1002/qj.828.

Deremble, B., G. Lapeyre, and M. Ghil, 2012: Atmospheric dynamics triggered by an oceanic SST front in a moist quasigeostrophic model. *J. Atmos. Sci.*, **69**, 1617–1632, https://doi.org/10.1175/JAS-D-11-0288.1.

Deser, C., M. A. Alexander, and M. S. Timlin, 1999: Evidence for a Wind-Driven Intensification of the Kuroshio Current Extension from the 1970s to the 1980s. *J. Climate*, **12**, 1697–1706, https://doi.org/10.1175/1520-0442(1999)012<1697:EFAWDI>2.0.CO;2.

Deser, C., R. A. Tomas, and S. L. Peng, 2007: The transient atmospheric circulation response to North Atlantic SST and sea ice anomalies. *J. Climate*, **20**, 4751–4767, https://doi.org/10.1175/JCLI4278.1.

Dewar, W. K., 2003: Nonlinear midlatitude ocean adjustment. *J. Phys. Oceanogr.*, **33**, 1057–1082, https://doi.org/10.1175/1520-0485(2003)033<1057:NMOA>2.0.CO;2.

Dijkstra, H. A., and M. Ghil, 2005: Low-frequency variability of the large-scale ocean circulation: A dynamical systems

approach. *Rev. Geophys.*, **43**, RG3002, https://doi.org/10.1029/2002RG000122.

Ding, M. R., P. F. Lin, H. L. Liu, and F. Chai, 2018: Increased Eddy Activity in the Northeastern Pacific during 1993-2011. *J. Climate*, **31**, 387–399, https://doi.org/10.1175/JCLI-D-17-0309.1.

Dong, C. M., F. Nencioli, Y. Liu, and J. C. McWilliams, 2011: An automated approach to detect oceanic eddies from satellite remotely sensed sea surface temperature data. *IEEE Geoscience and Remote Sensing Letters*, **8**, 1055–1059, https://doi.org/10.1109/LGRS.2011.2155029.

Dong, C. M., J. C. McWilliams, Y. Liu, and D. K. Chen, 2014: Global heat and salt transports by eddy movement. *Nature Communications*, **5**, 3294, https://doi.org/10.1038/ncomms4294.

Eady, E. T., 1949: Long waves and cyclone waves. *Tellus*, **1**, 33–52, https://doi.org/10.1111/j.2153-3490.1949.tb01265.x.

Faghmous, J. H., I. Frenger, Y. S. Yao, R. Warmka, A. Lindell, and V. Kumar, 2015: A daily global mesoscale ocean eddy dataset from satellite altimetry. *Scientific Data*, **2**, 150028, https://doi.org/10.1038/sdata.2015.28.

Feliks, Y., M. Ghil, and E. Simonnet, 2004: Low-frequency variability in the midlatitude atmosphere induced by an oceanic thermal front. *J. Atmos. Sci.*, **61**, 961–981, https://doi.org/10.1175/1520-0469(2004)061<0961:LVITMA>2.0.CO;2.

Feliks, Y., M. Ghil, and E. Simonnet, 2007: Low-frequency variability in the midlatitude baroclinic atmosphere induced by an oceanic thermal front. *J. Atmos. Sci.*, **64**, 97–116, https://doi.org/10.1175/JAS3780.1.

Feliks, Y., M. Ghil, and A. W. Robertson, 2011: The atmospheric circulation over the North Atlantic as induced by the SST field. *J. Climate*, **24**, 522–542, https://doi.org/10.1175/2010JCLI3859.1.

Ferreira, D., and C. Frankignoul, 2005: The transient atmospheric response to midlatitude SST anomalies. *J. Climate*, **18**, 1049–1067, https://doi.org/10.1175/JCLI-3313.1.

Foussard, A., G. Lapeyre, and R. Plougonven, 2019: Storm track response to oceanic eddies in idealized atmospheric simulations. *J. Climate*, **32**, 445–463, https://doi.org/10.1175/JCLI-D-18-0415.1.

Frankignoul, C., 1985: Sea surface temperature anomalies, planetary waves, and air-sea feedback in the middle latitudes. *Rev. Geophys.*, **23**, 357–390, https://doi.org/10.1029/RG023i004p00357.

Frankignoul, C., and K. Hasselmann, 1977: Stochastic climate models, Part II Application to sea-surface temperature anomalies and thermocline variability. *Tellus*, **29**, 289–305, https://doi.org/10.1111/j.2153-3490.1977.tb00740.x.

Frankignoul, C., and N. Sennéchael, 2007: Observed influence of North Pacific SST anomalies on the atmospheric circulation. *J. Climate*, **20**, 592–606, https://doi.org/10.1175/JCLI4021.1.

Frankignoul, C., N. Chouaib, and Z. Y. Liu, 2011a: Estimating the observed atmospheric response to SST anomalies: Maximum covariance analysis, generalized equilibrium feedback assessment, and maximum response estimation. *J. Climate*, **24**, 2523–2539, https://doi.org/10.1175/2010JCLI3696.1.

Frankignoul, C., N. Sennéchael, Y. O. Kwon, and M. A. Alexander, 2011b: Influence of the meridional shifts of the Kuroshio and the Oyashio extensions on the atmospheric circulation. *J. Climate*, **24**, 762–777, https://doi.org/10.1175/2010JCLI3731.1.

Frenger, I., N. Gruber, R. Knutti, and M. Münnich, 2013: Imprint of southern Ocean eddies on winds, clouds and rainfall. *Nature Geoscience*, **6**, 608–612, https://doi.org/10.1038/ngeo1863.

Gan, B. L., and L. X. Wu, 2013: Seasonal and long-term coupling between wintertime storm tracks and sea surface temperature in the North Pacific. *J. Climate*, **26**, 6123–6136, https://doi.org/10.1175/JCLI-D-12-00724.1.

Gan, B. L., L. X. Wu, F. Jia, S. J. Li, W. J. Cai, H. Nakamura, M. A. Alexander, and A. J. Miller, 2017: On the response of the aleutian low to greenhouse warming. *J. Climate*, **30**, 3907–3925, https://doi.org/10.1175/JCLI-D-15-0789.1.

Gao, J. X., R. H. Zhang, and H. N. Wang, 2019: Mesoscale SST perturbation-induced impacts on climatological precipitation in the Kuroshio-Oyashio extension region, as revealed by the WRF simulations. *Journal of Oceanology and Limnology*, **37**, 385–397, https://doi.org/10.1007/s00343-019-8065-5.

Gentile, V., S. Pierini, P. de Ruggiero, and L. Pietranera, 2018: Ocean modelling and altimeter data reveal the possible occurrence of intrinsic low-frequency variability of the Kuroshio Extension. *Ocean Modelling*, **131**, 24–39, https://doi.org/10.1016/j.ocemod.2018.08.006.

Graff, L. S., and J. H. LaCasce, 2012: Changes in the extratropical storm tracks in response to changes in SST in an AGCM. *J. Climate*, **25**, 1854–1870, https://doi.org/10.1175/JCLI-D-11-00174.1.

Hall, N. M. J., J. Derome, and H. Lin, 2001: The extratropical signal generated by a midlatitude SST anomaly. Part I: Sensitivity at equilibrium. *J. Climate*, **14**, 2035–2053, https://doi.org/10.1175/1520-0442(2001)014<2035:TESGBA>2.0.CO;2.

Hare, S. R., and N. J. Mantua, 2000: Empirical evidence for North Pacific regime shifts in 1977 and 1989. *Progress in Oceanography*, **47**, 103–145, https://doi.org/10.1016/S0079-6611(00)00033-1.

Hashizume, H., S. P. Xie, W. T. Liu, and K. Takeuchi, 2001: Local and remote atmospheric response to tropical instability waves: A global view from space. *J. Geophys. Res.: Atmos.*, **106**, 10 173–10 185, https://doi.org/10.1029/2000JD900684.

Hasselmann, K., 1976: Stochastic climate models Part I. *Theory. Tellus*, **28**, 473–485, https://doi.org/10.1111/j.2153-3490.1976.tb00696.x.

Hendon, H. H., and D. L. Hartmann, 1982: Stationary waves on a sphere: Sensitivity to thermal feedback. *J. Atmos. Sci.*, **39**, 1906–1920, https://doi.org/10.1175/1520-0469(1982)039<1906:SWOASS>2.0.CO;2.

Hersbach, H., and Coauthors, 2020: The ERA5 global reanalysis. *Quart. J. Roy. Meteor. Soc.*, **146**, 1999–2049, https://doi.org/10.1002/qj.3803.

Hirata, H., R. Kawamura, M. Kato, and T. Shinoda, 2015: Influential role of moisture supply from the Kuroshio/Kuroshio Extension in the rapid development of an extratropical cyclone. *Mon. Wea. Rev.*, **143**, 4126–4144, https://doi.org/10.1175/MWR-D-15-0016.1.

Hirata, H., R. Kawamura, M. Kato, and T. Shinoda, 2016: Response of rapidly developing extratropical cyclones to sea surface temperature variations over the western Kuroshio-Oyashio confluence region. *J. Geophys. Res.: Atmos.*, **121**, 3843–3858, https://doi.org/10.1002/2015JD024391.

Hirata, H., R. Kawamura, M. Kato, and T. Shinoda, 2018: A positive feedback process related to the rapid development of an extratropical cyclone over the Kuroshio/Kuroshio Extension. *Mon. Wea. Rev.*, **146**, 417–433, https://doi.org/10.1175/MWR-D-17-0063.1.

Hogg, A. M. C., P. D. Killworth, J. R. Blundell, and W. K. Dewar, 2005: Mechanisms of decadal variability of the wind-driven ocean circulation. *J. Phys. Oceanogr.*, **35**, 512–531, https://doi.org/10.1175/JPO2687.1.

Honda, M., and H. Nakamura, 2001: Interannual seesaw between the Aleutian and Icelandic lows. Part II: Its significance in the interannual variability over the wintertime northern hemisphere. *J. Climate*, **14**, 4512–4529, https://doi.org/10.1175/1520-0442(2001)014<4512:ISBTAA>2.0.CO;2.

Honda, M., H. Nakamura, J. Ukita, I. Kousaka, and K. Takeuchi, 2001: Interannual seesaw between the Aleutian and Icelandic lows. Part I: Seasonal dependence and life cycle. *J. Climate*, **14**, 1029–1042, https://doi.org/10.1175/1520-0442(2001)014<1029:ISBTAA>2.0.CO;2.

Honda, M., Y. Kushnir, H. Nakamura, S. Yamane, and S. E. Zebiak, 2005: Formation, mechanisms, and predictability of the Aleutian-Icelandic low seesaw in ensemble AGCM simulations. *J. Climate*, **18**, 1423–1434, https://doi.org/10.1175/JCLI3353.1.

Hoskins, B., M. Pedder, and D. W. Jones, 2003: The omega equation and potential vorticity. *Quart. J. Roy. Meteor. Soc.*, **129**, 3277–3303, https://doi.org/10.1256/qj.02.135.

Hoskins, B. J., 1983: Modelling of the transient eddies and their feedback on the mean flow. *Large-scale Dynamical Processes in the Atmosphere*, B. J. Hoskins and R. P. Pearce, Eds., Academic Press, 169–199.

Hoskins, B. J., and D. J. Karoly, 1981: The steady linear response of a spherical atmosphere to thermal and orographic forcing. *J. Atmos. Sci.*, **38**, 1179–1196, https://doi.org/10.1175/1520-0469(1981)038<1179:TSLROA>2.0.CO;2.

Hoskins, B. J., and P. J. Valdes, 1990: On the existence of storm-tracks. *J. Atmos. Sci.*, **47**, 1854–1864, https://doi.org/10.1175/1520-0469(1990)047<1854:OTEOST>2.0.CO;2.

Hoskins, B. J., and T. Ambrizzi, 1993: Rossby wave propagation on a realistic longitudinally varying flow. *J. Atmos. Sci.*, **50**, 1661–1671, https://doi.org/10.1175/1520-0469(1993)050<1661:RWPOAR>2.0.CO;2.

Hoskins, B. J., I. N. James, and G. H. White, 1983: The shape, propagation and mean-flow interaction of large-scale weather systems. *J. Atmos. Sci.*, **40**, 1595–1612, https://doi.org/10.1175/1520-0469(1983)040<1595:TSPAMF>2.0.CO;2.

Hotta, D., and H. Nakamura, 2011: On the significance of the sensible heat supply from the ocean in the maintenance of the mean baroclinicity along storm tracks. *J. Climate*, **24**, 3377–3401, https://doi.org/10.1175/2010JCLI3910.1.

Inatsu, M., and J. B. Hoskins, 2004: The zonal asymmetry of the southern hemisphere winter storm track. *J. Climate*, **17**, 4882–4892, https://doi.org/10.1175/JCLI-3232.1.

Isoguchi, O., H. Kawamura, and E. Oka, 2006: Quasi-stationary jets transporting surface warm waters across the transition zone between the subtropical and the subarctic gyres in the North Pacific. *J. Geophys. Res.: Oceans*, **111**, C10003, https://doi.org/10.1029/2005JC003402.

Iwao, K., M. Inatsu, and M. Kimoto, 2012: Recent changes in explosively developing extratropical cyclones over the winter northwestern Pacific. *J. Climate*, **25**, 7282–7296, https://doi.org/10.1175/JCLI-D-11-00373.1.

Jia, Y. L., P. Chang, I. Szunyogh, R. Saravanan, and J. T. Bacmeister, 2019: A modeling strategy for the investigation of the effect of mesoscale SST variability on atmospheric dynamics. *Geophys. Res. Lett.*, **46**, 3982–3989, https://doi.org/10.1029/2019GL081960.

Jiang, S., F. F. Jin, and M. Ghil, 1995: Multiple equilibria, periodic, and aperiodic solutions in a wind-driven, double-gyre, shallow-water model. *J. Phys. Oceanogr.*, **25**, 764–786, https://doi.org/10.1175/1520-0485(1995)025<0764:MEPAAS>2.0.CO;2.

Kaspi, Y., and T. Schneider, 2013: The role of stationary eddies in shaping midlatitude storm tracks. *J. Atmos. Sci.*, **70**, 2596–2613, https://doi.org/10.1175/JAS-D-12-082.1.

Kelly, K. A., R. J. Small, R. M. Samelson, B. Qiu, T. M. Joyce, Y. O. Kwon, and M. F. Cronin, 2010: Western boundary currents and frontal air-sea interaction: Gulf stream and Kuroshio Extension. *J. Climate*, **23**, 5644–5667, https://doi.org/10.1175/2010JCLI3346.1.

Kelly, P. M., and P. D. Jones, 1996: Removal of the El Niño-Southern Oscillation signal from the gridded surface air temperature data set. *J. Geophys. Res.*, **101**, 19 013–19 022, https://doi.org/10.1029/96JD01173.

Kida, S., and Coauthors, 2015: Oceanic fronts and jets around Japan: A review. *Journal of Oceanography*, **71**, 469–497, https://doi.org/10.1007/s10872-015-0283-7.

Kilpatrick, T., N. Schneider, and B. Qiu, 2014: Boundary layer convergence induced by strong winds across a midlatitude SST front. *J. Climate*, **27**, 1698–1718, https://doi.org/10.1175/JCLI-D-13-00101.1.

Kilpatrick, T., N. Schneider, and B. Qiu, 2016: Atmospheric response to a midlatitude SST front: Alongfront winds. *J. Atmos. Sci.*, **73**, 3489–3509, https://doi.org/10.1175/JAS-D-15-0312.1.

Kushnir, Y., W. A. Robinson, I. Bladé, N. M. J. Hall, S. Peng, and R. Sutton, 2002: Atmospheric GCM response to extratropical SST anomalies: Synthesis and evaluation. *J. Climate*, **15**, 2233–2256, https://doi.org/10.1175/1520-0442(2002)015<2233:AGRTES>2.0.CO;2.

Kuwano-Yoshida, A., and S. Minobe, 2017: Storm-track response to SST fronts in the northwestern Pacific region in an AGCM. *J. Climate*, **30**, 1081–1102, https://doi.org/10.1175/JCLI-D-16-0331.1.

Kuwano-Yoshida, A., T. Enomoto, and W. Ohfuchi, 2010: An improved PDF cloud scheme for climate simulations. *Quart. J. Roy. Meteor. Soc.*, **136**, 1583–1597, https://doi.org/10.1002/qj.660.

Kwon, Y. O., M. A. Alexander, N. A. Bond, C. Frankignoul, H. Nakamura, B. Qiu, and L. A. Thompson, 2010: Role of the Gulf Stream and Kuroshio-Oyashio Systems in large-scale atmosphere-ocean interaction: A review. *J. Climate*, **23**, 3249–3281, https://doi.org/10.1175/2010JCLI3343.1.

Lambaerts, J., G. Lapeyre, R. Plougonven, and P. Klein, 2013: Atmospheric response to sea surface temperature mesoscale structures. *J. Geophys. Res.: Atmos.*, **118**, 9611–9621, https://doi.org/10.1002/jgrd.50769.

Latif, M., and T. P. Barnett, 1994: Causes of decadal climate variability over the North Pacific and North America. *Science*, **266**, 634–637, https://doi.org/10.1126/science.266.5185.634.

Lee, S., and H. Kim, 2003: The dynamical relationship between subtropical and eddy-driven jets. *J. Atmos. Sci.*, **60**, 1490–1503, https://doi.org/10.1175/1520-0469(2003)060<14

90:TDRBSA>2.0.CO;2.

Lee, W. J., and M. Mak, 1996: The role of orography in the dynamics of storm tracks. *J. Atmos. Sci.*, **53**, 1737–1750, https://doi.org/10.1175/1520-0469(1996)053<1737:TROOIT>2.0.CO;2.

Leyba, I. M., M. Saraceno, and S. A. Solman, 2017: Air-sea heat fluxes associated to mesoscale eddies in the Southwestern Atlantic Ocean and their dependence on different regional conditions. *Climate Dyn.*, **49**, 2491–2501, https://doi.org/10.1007/s00382-016-3460-5.

Lindzen, R. S., and B. Farrell, 1980: A simple approximate result for the maximum growth rate of baroclinic instabilities. *J. Atmos. Sci.*, **37**, 1648–1654, https://doi.org/10.1175/1520-0469(1980)037<1648:ASARFT>2.0.CO;2.

Lindzen, R. S., and S. Nigam, 1987: On the role of sea surface temperature gradients in forcing low-level winds and convergence in the tropics. *J. Atmos. Sci.*, **44**, 2418–2436, https://doi.org/10.1175/1520-0469(1987)044<2418:OTROSS>2.0.CO;2.

Liu, J. W., S. P. Zhang, and S. P. Xie, 2013: Two types of surface wind response to the East China Sea Kuroshio front. *J. Climate*, **26**, 8616–8627, https://doi.org/10.1175/JCLI-D-12-00092.1.

Liu, Q. Y., N. Wen, and Z. Y. Liu, 2006: An observational study of the impact of the North Pacific SST on the atmosphere. *Geophys. Res. Lett.*, **33**, L18611, https://doi.org/10.1029/2006GL026082.

Liu, T. W., X. S. Xie, P. S. Polito, S. P. Xie, and H. Hashizume, 2000: Atmospheric manifestation of tropical instability wave observed by QuikSCAT and tropical rain measuring mission. *Geophys. Res. Lett.*, **27**, 2545–2548, https://doi.org/10.1029/2000GL011545.

Liu, X., and Coauthors, 2021: Ocean fronts and eddies force atmospheric rivers and heavy precipitation in western North America. *Nature Communications*, **12**, 1268, https://doi.org/10.1038/s41467-021-21504-w.

Liu, Z. Y., and E. Di Lorenzo, 2018: Mechanisms and predictability of Pacific decadal variability. *Current Climate Change Reports*, **4**, 128–144, https://doi.org/10.1007/s40641-018-0090-5.

Liu, Z. Y., Y. Liu, L. X. Wu, and R. Jacob, 2007: Seasonal and long-term atmospheric responses to reemerging North Pacific Ocean variability: A combined dynamical and statistical assessment. *J. Climate*, **20**, 955–980, https://doi.org/10.1175/JCLI4041.1.

Liu, Z. Y., L. Fan, S. I. Shin, and Q. Y. Liu, 2012a: Assessing atmospheric response to surface forcing in the observations. Part II: Cross validation of seasonal response using GEFA and LIM. *J. Climate*, **25**, 6817–6834, https://doi.org/10.1175/JCLI-D-11-00630.1.

Liu, Z. Y., N. Wen, and L. Fan, 2012b: Assessing atmospheric response to surface forcing in the observations. Part I: Cross validation of annual response using GEFA, LIM, and FDT. *J. Climate*, **25**, 6796–6816, https://doi.org/10.1175/JCLI-D-11-00545.1.

Lu, J., G. Chen, and D. M. W. Frierson, 2010: The position of the midlatitude storm track and eddy-driven westerlies in aquaplanet AGCMs. *J. Atmos. Sci.*, **67**, 3984–4000, https://doi.org/10.1175/2010JAS3477.1.

Luo, D. H., S. H. Feng, and L. X. Wu, 2016: The eddy-dipole mode interaction and the decadal variability of the Kuroshio Extension system. *Ocean Dynamics*, **66**, 1317–1332, https://doi.org/10.1007/s10236-016-0991-6.

Ma, J., H. M. Xu, C. M. Dong, P. F. Lin, and Y. Liu, 2015a: Atmospheric responses to oceanic eddies in the Kuroshio Extension region. *J. Geophys. Res.: Atmos.*, **120**, 6313–6330, https://doi.org/10.1002/2014JD022930.

Ma, X. H., and Coauthors, 2015b: Distant influence of Kuroshio eddies on North Pacific weather patterns? *Scientific Reports*, **5**, 17785, https://doi.org/10.1038/srep17785.

Ma, X. H., and Coauthors, 2016: Western boundary currents regulated by interaction between ocean eddies and the atmosphere. *Nature*, **535**, 533–537, https://doi.org/10.1038/nature18640.

Ma, X. H., P. Chang, R. Saravanan, R. Montuoro, H. Nakamura, D. X. Wu, X. P. Lin, and L. X. Wu, 2017: Importance of resolving Kuroshio front and eddy influence in simulating the North Pacific storm track. *J. Climate*, **30**, 1861–1880, https://doi.org/10.1175/JCLI-D-16-0154.1.

Marshall, J. C., and R. A. Plumb, 2008: *Atmosphere*, *Ocean and Climate Dynamics*: *An Introductory Text*. R. Dmowska, D. Hartmann, and H.T. Rossby, Eds. Elsevier Academic Press, London, 345 pp.

Masunaga, R., H. Nakamura, T. Miyasaka, K. Nishii, and Y. Tanimoto, 2015: Separation of climatological imprints of the Kuroshio Extension and Oyashio Fronts on the wintertime atmospheric boundary layer: Their sensitivity to SST resolution prescribed for atmospheric reanalysis. *J. Climate*, **28**, 1764–1787, https://doi.org/10.1175/JCLI-D-14-00314.1.

Masunaga, R., H. Nakamura, T. Miyasaka, K. Nishii, and B. Qiu, 2016: Interannual modulations of oceanic imprints on the wintertime atmospheric boundary layer under the changing dynamical regimes of the Kuroshio Extension. *J. Climate*, **29**, 3273–3296, https://doi.org/10.1175/JCLI-D-15-0545.1.

Masunaga, R., H. Nakamura, B. Taguchi, and T. Miyasaka, 2020a: Processes shaping the frontal-scale time-mean surface wind convergence patterns around the Kuroshio Extension in winter. *J. Climate*, **33**, 3–25, https://doi.org/10.1175/JCLI-D-19-0097.1.

Masunaga, R., H. Nakamura, B. Taguchi, and T. Miyasaka, 2020b: Processes shaping the frontal-scale time-mean surface wind convergence patterns around the Gulf Stream and Agulhas Return Current in winter. *J. Climate*, **33**, 9083–9101, https://doi.org/10.1175/JCLI-D-19-0948.1.

McCalpin, J. D., and D. B. Haidvogel, 1996: Phenomenology of the low-frequency variability in a reduced-gravity, quasigeostrophic double-gyre model. *J. Phys. Oceanogr.*, **26**, 739–752, https://doi.org/10.1175/1520-0485(1996)026<0739:POTLFV>2.0.CO;2.

McWilliams, J. C., 2016: Submesoscale currents in the ocean. *Proceedings of the Royal Society A: Mathematical, Physical and Engineering Sciences*, **472**, 20160117, https://doi.org/10.1098/rspa.2016.0117.

Michel, C., and G. Rivière, 2014: Sensitivity of the position and variability of the eddy-driven jet to different SST profiles in an aquaplanet general circulation model. *J. Atmos. Sci.*, **71**, 349–371, https://doi.org/10.1175/JAS-D-13-074.1.

Miller, A. J., D. R. Cayan, and W. B. White, 1998: A westward-intensified decadal change in the North Pacific thermocline and gyre-scale circulation. *J. Climate*, **11**, 3112–3127, https://doi.org/10.1175/1520-0442(1998)011<3112:AWIDCI>2.0.CO;2.

Minobe, S., A. Kuwano-Yoshida, N. Komori, S. P. Xie, and R. J. Small, 2008: Influence of the Gulf Stream on the tropo-

sphere. *Nature*, **452**, 206–209, https://doi.org/10.1038/nature06690.

Minobe, S., M. Miyashita, A. Kuwano-Yoshida, H. Tokinaga, and S. P. Xie, 2010: Atmospheric response to the Gulf Stream: Seasonal variations. *J. Climate*, **23**, 3699–3719, https://doi.org/10.1175/2010JCLI3359.1.

Miyama, T., M. Nonaka, H. Nakamura, and A. Kuwano-Yoshida, 2012: A striking early-summer event of a convective rainband persistent along the warm Kuroshio in the East China Sea. *Tellus A: Dynamic Meteorology and Oceanography*, **64**, 18962, https://doi.org/10.3402/tellusa.v64i0.18962.

Mizuno, K., and W. B. White, 1983: Annual and interannual variability in the Kuroshio current system. *J. Phys. Oceanogr.*, **13**, 1847–1867,https://doi.org/10.1175/1520-0485(1983)013<1847:AAIVIT>2.0.CO;2.

Nakamura, H., and A. S. Kazmin, 2003: Decadal changes in the North Pacific oceanic frontal zones as revealed in ship and satellite observations. *J. Geophys. Res.*, **108**, 3078, https://doi.org/10.1029/1999JC000085.

Nakamura, M., and S. Yamane, 2009: Dominant anomaly patterns in the near-surface baroclinicity and accompanying anomalies in the atmosphere and oceans. Part I: North Atlantic basin. *J. Climate*, **22**, 880–904, https://doi.org/10.1175/2008JCLI2297.1.

Nakamura, M., and S. Yamane, 2010: Dominant anomaly patterns in the near-surface baroclinicity and accompanying anomalies in the atmosphere and oceans. Part II: North Pacific basin. *J. Climate*, **23**, 6445–6467, https://doi.org/10.1175/2010JCLI3017.1.

Nakamura, M., and T. Miyama, 2014: Impacts of the Oyashio temperature front on the regional climate. *J. Climate*, **27**, 7861–7873, https://doi.org/10.1175/JCLI-D-13-00609.1.

Nakamura, H., T. Sampe, Y. Tanimoto, and A. Shimpo, 2004: Observed associations among storm tracks, jet streams and midlatitude oceanic fronts. *Earth's Climate*: *The Ocean-Atmosphere Interaction*, C. Wang, S. P. Xie, and J. A. Carton, Eds., American Geophysical Union, 147: 329–346, https://doi.org/10.1029/147GM18.

Nakamura, H., T. Sampe, A. Goto, W. Ohfuchi, and S. P. Xie, 2008: On the importance of midlatitude oceanic frontal zones for the mean state and dominant variability in the tropospheric circulation. *Geophys. Res. Lett.*, **35**, L15709, https://doi.org/10.1029/2008GL034010.

Nakano, H., H. Tsujino, K. Sakamoto, S. Urakawa, T. Toyoda, and G. Yamanaka, 2018: Identification of the fronts from the Kuroshio Extension to the Subarctic Current using absolute dynamic topographies in satellite altimetry products. *Journal of Oceanography*, **74**, 393–420, https://doi.org/10.1007/s10872-018-0470-4.

Newman, P. A., L. Coy, S. Pawson, and L. R. Lait, 2016: The anomalous change in the QBO in 2015-2016. *Geophys. Res. Lett.*, **43**, 8791–8797, https://doi.org/10.1002/2016GL070373.

Nkwinkwa Njouodo, A. S. N., S. Koseki, N. Keenlyside, and M. Rouault, 2018: Atmospheric signature of the Agulhas Current. *Geophys. Res. Lett.*, **45**, 5185–5193, https://doi.org/10.1029/2018GL077042.

Nonaka, M., and S. P. Xie, 2003: Covariations of sea surface temperature and wind over the Kuroshio and its extension: Evidence for ocean-to-atmosphere feedback. *J. Climate*, **16**, 1404–1413, https://doi.org/10.1175/1520-0442(2003)16<1404:COSSTA>2.0.CO;2.

Nonaka, M., H. Nakamura, Y. Tanimoto, T. Kagimoto, and H. Sasaki, 2006: Decadal variability in the Kuroshio-Oyashio Extension simulated in an eddy-resolving OGCM. *J. Climate*, **19**, 1970–1989, https://doi.org/10.1175/JCLI3793.1.

Nonaka, M., H. Nakamura, Y. Tanimoto, T. Kagimoto, and H. Sasaki, 2008: Interannual-to-decadal variability in the Oyashio and its influence on temperature in the subarctic frontal zone: An eddy-resolving OGCM simulation. *J. Climate*, **21**, 6283–6303, https://doi.org/10.1175/2008JCLI2294.1.

Nonaka, M., H. Nakamura, B. Taguchi, N. Komori, A. Kuwano-Yoshida, and K. Takaya, 2009: Air-sea heat exchanges characteristic of a prominent midlatitude oceanic front in the South Indian Ocean as simulated in a high-resolution coupled GCM. *J. Climate*, **22**, 6515–6535, https://doi.org/10.1175/2009JCLI2960.1.

Nonaka, M., H. Sasaki, B. Taguchi, and N. Schneider, 2020: Atmospheric-driven and intrinsic interannual-to-decadal variability in the Kuroshio Extension jet and eddy activities. *Frontiers in Marine Science*, **7**, 547442, https://doi.org/10.3389/fmars.2020.547442.

O'Neill, L. W., 2012: Wind speed and stability effects on coupling between surface wind stress and SST observed from buoys and satellite. *J. Climate*, **25**, 1544–1569, https://doi.org/10.1175/JCLI-D-11-00121.1.

O'Neill, L. W., D. B. Chelton, and S. K. Esbensen, 2003: Observations of SST-induced perturbations of the wind stress field over the Southern Ocean on seasonal timescales. *J. Climate*, **16**, 2340–2354, https://doi.org/10.1175/2780.1.

O'Neill, L. W., D. B. Chelton, S. K. Esbensen, and F. J. Wentz, 2005: High-resolution satellite measurements of the atmospheric boundary layer response to SST variations along the Agulhas Return Current. *J. Climate*, **18**, 2706–2723, https://doi.org/10.1175/JCLI3415.1.

O'Neill, L. W., S. K. Esbensen, N. Thum, R. M. Samelson, and D. B. Chelton, 2010: Dynamical analysis of the boundary layer and surface wind responses to mesoscale SST perturbations. *J. Climate*, **23**, 559–581, https://doi.org/10.1175/2009JCLI2662.1.

O'Reilly, C. H., and A. Czaja, 2015: The response of the Pacific storm track and atmospheric circulation to Kuroshio Extension variability. *Quart. J. Roy. Meteor. Soc.*, **141**, 52–66, https://doi.org/10.1002/qj.2334.

O'Neill, L. W., T. Haack, D. B. Chelton, and E. Skyllingstad, 2017: The Gulf Stream convergence zone in the time-mean winds. *J. Atmos. Sci.*, **74**, 2383–2412, https://doi.org/10.1175/JAS-D-16-0213.1.

O'Neill, L. W., T. Haack, D. B. Chelton, and E. Skyllingstad, 2018: Reply to "Comments on 'The Gulf Stream Convergence Zone in the Time-Mean Winds.'". *J. Atmos. Sci.*, **75**, 2151–2153, https://doi.org/10.1175/JAS-D-18-0044.1.

Ogawa, F., H. Nakamura, K. Nishii, T. Miyasaka, and A. Kuwano-Yoshida, 2012: Dependence of the climatological axial latitudes of the tropospheric westerlies and storm tracks on the latitude of an extratropical oceanic front. *Geophys. Res. Lett.*, **39**, L05804, https://doi.org/10.1029/2011GL049922.

Okajima, S., H. Nakamura, K. Nishii, T. Miyasaka, and A. Kuwano-Yoshida, 2014: Assessing the importance of prominent warm SST anomalies over the midlatitude North Pacific in forcing large-scale atmospheric anomalies during 2011 summer and autumn. *J. Climate*, **27**, 3889–3903, https://doi.org/

10.1175/JCLI-D-13-00140.1.

Okajima, S., H. Nakamura, K. Nishii, T. Miyasaka, A. Kuwano-Yoshida, B. Taguchi, M. Mori, and Y. Kosaka, 2018: Mechanisms for the maintenance of the wintertime basin-scale atmospheric response to decadal SST variability in the North Pacific subarctic frontal zone. *J. Climate*, **31**, 297–315, https://doi.org/10.1175/JCLI-D-17-0200.1.

Palmer, T. N., and Z. B. Sun, 1985: A modelling and observational study of the relationship between sea surface temperature in the north-west Atlantic and the atmospheric general circulation. *Quart. J. Roy. Meteor. Soc.*, **111**, 947–975, https://doi.org/10.1256/smsqj.47002.

Papritz, L., and T. Spengler, 2015: Analysis of the slope of isentropic surfaces and its tendencies over the North Atlantic. *Quart. J. Roy. Meteor. Soc.*, **141**, 3226–3238, https://doi.org/10.1002/qj.2605.

Parfitt, R., and A. Czaja, 2016: On the contribution of synoptic transients to the mean atmospheric state in the Gulf Stream region. *Quart. J. Roy. Meteor. Soc.*, **142**, 1554–1561, https://doi.org/10.1002/qj.2689.

Parfitt, R., and H. Seo, 2018: A new framework for near-surface wind convergence over the Kuroshio Extension and Gulf Stream in wintertime: The role of atmospheric fronts. *Geophys. Res. Lett.*, **45**, 9909–9918, https://doi.org/10.1029/2018GL080135.

Parfitt, R., A. Czaja, S. Minobe, and A. Kuwano-Yoshida, 2016: The atmospheric frontal response to SST perturbations in the Gulf Stream region. *Geophys. Res. Lett.*, **43**, 2299–2306, https://doi.org/10.1002/2016GL067723.

Parfitt, R., A. Czaja, and Y. O. Kwon, 2017: The impact of SST resolution change in the ERA-Interim reanalysis on wintertime Gulf Stream frontal air-sea interaction. *Geophys. Res. Lett.*, **44**, 3246–3254, https://doi.org/10.1002/2017GL073028.

Peng, S. L., and J. S. Whitaker, 1999: Mechanisms determining the atmospheric response to midlatitude SST anomalies. *J. Climate*, **12**, 1393–1408, https://doi.org/10.1175/1520-0442(1999)012<1393:MDTART>2.0.CO;2.

Peng, S. L., L. A. Mysak, J. Derome, H. Ritchie, and B. Dugas, 1995: The difference between early and middle winter atmospheric response to sea surface temperature anomalies in the northwest Atlantic. *J. Climate*, **8**, 137–157, https://doi.org/10.1175/1520-0442(1995)008<0137:TDBEAM>2.0.CO;2.

Peng, S. L., W. A. Robinson, and M. P. Hoerling, 1997: The modeled atmospheric response to midlatitude SST anomalies and its dependence on background circulation states. *J. Climate*, **10**, 971–987, https://doi.org/10.1175/1520-0442(1997)010<0971:TMARTM>2.0.CO;2.

Perlin, N., S. P. de Szoeke, D. B. Chelton, R. M. Samelson, E. D. Skyllingstad, and L. W. O'Neill, 2014: Modeling the atmospheric boundary layer wind response to mesoscale sea surface temperature perturbations. *Mon. Wea. Rev.*, **142**, 4284–4307, https://doi.org/10.1175/MWR-D-13-00332.1.

Pierini, S., 2006: A Kuroshio Extension system model study: Decadal chaotic self-sustained oscillations. *J. Phys. Oceanogr.*, **36**, 1605–1625, https://doi.org/10.1175/JPO2931.1.

Pierini, S., 2010: Coherence resonance in a double-gyre model of the Kuroshio Extension. *J. Phys. Oceanogr.*, **40**, 238–248, https://doi.org/10.1175/2009JPO4229.1.

Pierini, S., 2011: Low-frequency variability, coherence resonance, and phase selection in a low-order model of the wind-driven ocean circulation. *J. Phys. Oceanogr.*, **41**, 1585–1604, https://doi.org/10.1175/JPO-D-10-05018.1.

Pierini, S., 2014: Kuroshio extension bimodality and the North Pacific oscillation: A case of intrinsic variability paced by external forcing. *J. Climate*, **27**, 448–454, https://doi.org/10.1175/JCLI-D-13-00306.1.

Plougonven, R., A. Foussard, and G. Lapeyre, 2018: Comments on "The Gulf Stream Convergence Zone in the Time-Mean Winds." *J. Atmos. Sci.*, **75**, 2139–2149, https://doi.org/10.1175/JAS-D-17-0369.1.

Primeau, F., and D. Newman, 2008: Elongation and contraction of the western boundary current extension in a shallow-water model: A bifurcation analysis. *J. Phys. Oceanogr.*, **38**, 1469–1485, https://doi.org/10.1175/2007JPO3658.1.

Putrasahan, D. A., I. Kamenkovich, M. Le Hénaff, and B. P. Kirtman, 2017: Importance of ocean mesoscale variability for air-sea interactions in the Gulf of Mexico. *Geophys. Res. Lett.*, **44**, 6352–6362, https://doi.org/10.1002/2017GL072884.

Qiu, B., 2001: Kuroshio and Oyashio currents. *Encyclopedia of Ocean Sciences*. Academic Press, 1413–1425.

Qiu, B., 2002: Large-scale variability in the midlatitude subtropical and subpolar North Pacific ocean: Observations and causes. *J. Phys. Oceanogr.*, **32**, 353–375, https://doi.org/10.1175/1520-0485(2002)032<0353:LSVITM>2.0.CO;2.

Qiu, B., 2003: Kuroshio extension variability and forcing of the pacific decadal oscillations: Responses and potential feedback. *J. Phys. Oceanogr.*, **33**, 2465–2482, https://doi.org/10.1175/2459.1.

Qiu, B., and W. F. Miao, 2000: Kuroshio path variations south of Japan: Bimodality as a self-sustained internal oscillation. *J. Phys. Oceanogr.*, **30**, 2124–2137, https://doi.org/10.1175/1520-0485(2000)030<2124:KPVSOJ>2.0.CO;2.

Qiu, B., and S. M. Chen, 2005: Variability of the Kuroshio Extension jet, recirculation gyre, and mesoscale eddies on decadal time scales. *J. Phys. Oceanogr.*, **35**, 2090–2103, https://doi.org/10.1175/JPO2807.1.

Qiu, B., and S. M. Chen, 2006: Decadal variability in the formation of the North Pacific subtropical mode water: Oceanic versus atmospheric control. *J. Phys. Oceanogr.*, **36**, 1365–1380, https://doi.org/10.1175/JPO2918.1.

Qiu, B., and S. M. Chen, 2010: Eddy-mean flow interaction in the decadally modulating Kuroshio Extension system. *Deep Sea Research Part II: Topical Studies in Oceanography*, **57**, 1098–1110, https://doi.org/10.1016/j.dsr2.2008.11.036.

Qiu, B., N. Schneider, and S. M. Chen, 2007: Coupled decadal variability in the North Pacific: An observationally constrained idealized model. *J. Climate*, **20**, 3602–3620, https://doi.org/10.1175/JCLI4190.1.

Qiu, B., S. M. Chen, N. Schneider, and B. Taguchi, 2014: A coupled decadal prediction of the dynamic state of the Kuroshio Extension system. *J. Climate*, **27**, 1751–1764, https://doi.org/10.1175/JCLI-D-13-00318.1.

Qiu, B., S. M. Chen, P. Klein, C. Ubelmann, L. L. Fu, and H. Sasaki, 2016: Reconstructability of three-dimensional upper-ocean circulation from SWOT sea surface height measurements. *J. Phys. Oceanogr.*, **46**, 947–963, https://doi.org/10.1175/JPO-D-15-0188.1.

Qiu, B., S. M. Chen, and N. Schneider, 2017: Dynamical links between the decadal variability of the Oyashio and Kuroshio Extensions. *J. Climate*, **30**, 9591–9605, https://doi.org/10.1175/JCLI-D-17-0397.1.

Qiu, B., S. M. Chen, P. Klein, H. Torres, J. B. Wang, L. L. Fu, and D. Menemenlis, 2020a: Reconstructing upper-ocean ver-

tical velocity field from sea surface height in the presence of unbalanced motion. *J. Phys. Oceanogr.*, **50**, 55–79, https://doi.org/10.1175/JPO-D-19-0172.1.

Qiu, B., S. M. Chen, N. Schneider, E. Oka, and S. Sugimoto, 2020b: On the reset of the wind-forced decadal Kuroshio Extension variability in Late 2017. *J. Climate*, **33**, 10 813–10 828, https://doi.org/10.1175/JCLI-D-20-0237.1.

Renault, L., M. J. Molemaker, J. C. McWilliams, A. F. Shchepetkin, F. Lemarié, D. Chelton, S. Illig, and A. Hall, 2016: Modulation of wind work by oceanic current interaction with the atmosphere. *J. Phys. Oceanogr.*, **46**, 1685–1704, https://doi.org/10.1175/JPO-D-15-0232.1.

Renault, L., P. Marchesiello, S. Masson, and J. C. McWilliams, 2019: Remarkable control of western boundary currents by *Eddy Killing*, a mechanical air-sea coupling process. *Geophys. Res. Lett.*, **46**, 2743–2751, https://doi.org/10.1029/2018GL081211.

Révelard, A., C. Frankignoul, N. Sennéchael, Y. O. Kwon, and B. Qiu, 2016: Influence of the decadal variability of the Kuroshio Extension on the atmospheric circulation in the cold season. *J. Climate*, **29**, 2123–2144, https://doi.org/10.1175/JCLI-D-15-0511.1.

Rocha, C. B., T. K. Chereskin, S. T. Gille, and D. Menemenlis, 2016: Mesoscale to submesoscale wavenumber spectra in drake passage. *J. Phys. Oceanogr.*, **46**, 601–620, https://doi.org/10.1175/JPO-D-15-0087.1.

Rouault, M., P. Verley, and B. Backeberg, 2016: Wind changes above warm Agulhas Current eddies. *Ocean Scirnvr*, **12**, 495–506, https://doi.org/10.5194/os-12-495-2016.

Sampe, T., H. Nakamura, A. Goto, and W. Ohfuchi, 2010: Significance of a midlatitude SST frontal zone in the formation of a storm track and an eddy-driven westerly Jet. *J. Climate*, **23**, 1793–1814, https://doi.org/10.1175/2009JCLI3163.1.

Sardeshmukh, P. D., and B. J. Hoskins, 1988: The generation of global rotational flow by steady idealized tropical divergence. *J. Atmos. Sci.*, **45**, 1228–1251, https://doi.org/10.1175/1520-0469(1988)045<1228:TGOGRF>2.0.CO;2.

Sasaki, Y. N., S. Minobe, T. Asai, and M. Inatsu, 2012: Influence of the Kuroshio in the East China Sea on the early summer (Baiu) rain. *J. Climate*, **25**, 6627–6645, https://doi.org/10.1175/JCLI-D-11-00727.1.

Saulière, J., D. J. Brayshaw, B. Hoskins, and M. Blackburn, 2012: Further investigation of the impact of idealized continents and SST distributions on the northern hemisphere storm tracks. *J. Atmos. Sci.*, **69**, 840–856, https://doi.org/10.1175/JAS-D-11-0113.1.

Schultz, D. M., and Coauthors, 2019: Extratropical cyclones: A century of research on meteorology's centerpiece. *Meteor. Monogr.*, **59**, 16.1–16.56, https://doi.org/10.1175/AMSMONOGRAPHS-D-18-0015.1.

Seager, R., Y. Kushnir, N. H. Naik, M. A. Cane, and J. Miller, 2001: Wind-driven shifts in the latitude of the Kuroshio-Oyashio Extension and generation of SST anomalies on decadal timescales. *J. Climate*, **14**, 4249–4265, https://doi.org/10.1175/1520-0442(2001)014<4249:WDSITL>2.0.CO;2.

Seo, Y., S. Sugimoto, and K. Hanawa, 2014: Long-term variations of the Kuroshio Extension path in winter: Meridional movement and path state change. *J. Climate*, **27**, 5929–5940, https://doi.org/10.1175/JCLI-D-13-00641.1.

Sheldon, L., A. Czaja, B. Vannière, C. Morcrette, B. Sohet, M. Casado, and D. Smith, 2017: A 'warm path' for Gulf Stream-troposphere interactions. *Tellus A: Dynamic Meteorology and Oceanography*, **69**, 1299397, https://doi.org/10.1080/16000870.2017.1299397.

Shimada, T., and S. Minobe, 2011: Global analysis of the pressure adjustment mechanism over sea surface temperature fronts using AIRS/Aqua data. *Geophys. Res. Lett.*, **38**, L06704, https://doi.org/10.1029/2010GL046625.

Skyllingstad, E. D., D. Vickers, L. Mahrt, and R. Samelson, 2007: Effects of mesoscale sea-surface temperature fronts on the marine atmospheric boundary layer. *Bound.-Layer Meteor.*, **123**, 219–237, https://doi.org/10.1007/s10546-006-9127-8.

Small, R. J., and Coauthors, 2008: Air-sea interaction over ocean fronts and eddies. *Dyn. Atmos. Oceans*, **45**, 274–319, https://doi.org/10.1016/j.dynatmoce.2008.01.001.

Small, R. J., R. A. Tomas, and F. O. Bryan, 2014: Storm track response to ocean fronts in a global high-resolution climate model. *Climate Dyn.*, **43**, 805–828, https://doi.org/10.1007/s00382-013-1980-9.

Small, R. J., R. Msadek, Y. O. Kwon, J. F. Booth, and C. Zarzycki, 2019: Atmosphere surface storm track response to resolved ocean mesoscale in two sets of global climate model experiments. *Climate Dyn.*, **52**, 2067–2089, https://doi.org/10.1007/s00382-018-4237-9.

Smirnov, D., M. Newman, M. A. Alexander, Y. O. Kwon, and C. Frankignoul, 2015: Investigating the local atmospheric response to a realistic shift in the Oyashio sea surface temperature front. *J. Climate*, **28**, 1126–1147, https://doi.org/10.1175/JCLI-D-14-00285.1.

Stephenson, G. R., S. T. Gille, and J. Sprintall, 2013: Processes controlling upper-ocean heat content in Drake Passage. *J. Geophys. Res.: Oceans*, **118**, 4409–4423, https://doi.org/10.1002/jgrc.20315.

Stevens, B., and Coauthors, 2019: DYAMOND: The DYnamics of the atmospheric general circulation modeled on non-hydrostatic domains. *Progress in Earth and Planetary Science*, **6**, 61, https://doi.org/10.1186/s40645-019-0304-z.

Stoelinga, M. T., 1996: A potential vorticity-based study of the role of diabatic heating and friction in a numerically simulated baroclinic cyclone. *Mon. Wea. Rev.*, **124**, 849–874, https://doi.org/10.1175/1520-0493(1996)124<0849:APVBSO>2.0.CO;2.

Stull, R., 2017: *Practical Meteorology*: *An Algebra-based Survey of Atmospheric Science*. University of British Columbia, 940 pp.

Sugimoto, S., and K. Hanawa, 2009: Decadal and interdecadal variations of the aleutian low activity and their relation to upper oceanic variations over the North Pacific. *J. Meteor. Soc. Japan Ser II*, **87**, 601–614, https://doi.org/10.2151/jmsj.87.601.

Sugimoto, S., and K. Hanawa, 2011: Roles of SST anomalies on the wintertime turbulent heat fluxes in the Kuroshio-Oyashio Confluence region: Influences of warm eddies detached from the Kuroshio Extension. *J. Climate*, **24**, 6551–6561, https://doi.org/10.1175/2011JCLI4023.1.

Sugimoto, S., N. Kobayashi, and K. Hanawa, 2014: Quasi-decadal variation in intensity of the western part of the winter subarctic SST front in the western North Pacific: The influence of Kuroshio Extension path state. *J. Phys. Oceanogr.*, **44**, 2753–2762, https://doi.org/10.1175/JPO-D-13-0265.1.

Sugimoto, S., K. Aono, and S. Fukui, 2017: Local atmospheric response to warm mesoscale ocean eddies in the Kuroshio-

Oyashio Confluence region. *Scientific Reports*, **7**, 11871, https://doi.org/10.1038/s41598-017-12206-9.

Sun, X. G., L. F. Tao, and X. Q. Yang, 2018: The influence of oceanic stochastic forcing on the atmospheric response to midlatitude North Pacific SST anomalies. *Geophys. Res. Lett.*, **45**, 9297–9304, https://doi.org/10.1029/2018GL078860.

Taguchi, B., S. P. Xie, H. Mitsudera, and A. Kubokawa, 2005: Response of the Kuroshio Extension to rossby waves associated with the 1970s climate regime shift in a high-resolution ocean model. *J. Climate*, **18**, 2979–2995, https://doi.org/10.1175/JCLI3449.1.

Taguchi, B., S. P. Xie, N. Schneider, M. Nonaka, H. Sasaki, and Y. Sasai, 2007: Decadal variability of the Kuroshio Extension: Observations and an eddy-resolving model hindcast. *J. Climate*, **20**, 2357–2377, https://doi.org/10.1175/JCLI4142.1.

Taguchi, B., H. Nakamura, M. Nonaka, and S. P. Xie, 2009: Influences of the Kuroshio/Oyashio Extensions on air-sea heat exchanges and storm-track activity as revealed in regional atmospheric model simulations for the 2003/04 cold season. *J. Climate*, **22**, 6536–6560, https://doi.org/10.1175/2009JCLI2910.1.

Taguchi, B., H. Nakamura, M. Nonaka, N. Komori, A. Kuwano-Yoshida, K. Takaya, and A. Goto, 2012: Seasonal evolutions of atmospheric response to decadal SST anomalies in the North Pacific subarctic frontal zone: Observations and a coupled model simulation. *J. Climate*, **25**, 111–139, https://doi.org/10.1175/JCLI-D-11-00046.1.

Thomas, L. N., A. Tandon, and A. Mahadevan, 2008: Submesoscale processes and dynamics. *Ocean Modeling in an Eddying Regime*, M. W. Hecht and H. Hasumi, Eds., American Geophysical Union, 177: 17–38.

Tian, F. X., J. S. von Storch, and E. Hertwig, 2017: Air-sea fluxes in a climate model using hourly coupling between the atmospheric and the oceanic components. *Climate Dyn.*, **48**, 2819–2836, https://doi.org/10.1007/s00382-016-3228-y.

Tierney, G., D. J. Posselt, and J. F. Booth, 2018: An examination of extratropical cyclone response to changes in baroclinicity and temperature in an idealized environment. *Climate Dyn.*, **51**, 3829–3846, https://doi.org/10.1007/s00382-018-4115-5.

Ting, M. F., 1991: The stationary wave response to a midlatitude SST anomaly in an idealized GCM. *J. Atmos. Sci.*, **48**, 1249–1275, https://doi.org/10.1175/1520-0469(1991)048<1249:TSWRTA>2.0.CO;2.

Ting, M. F., and S. L. Peng, 1995: Dynamics of the early and middle winter atmospheric responses to the northwest Atlantic SST anomalies. *J. Climate*, **8**, 2239–2254, https://doi.org/10.1175/1520-0442(1995)008<2239:DOTEAM>2.0.CO;2.

Tokinaga, H., Y. Tanimoto, and S. P. Xie, 2005: SST-induced surface wind variations over the Brazil-Malvinas Confluence: Satellite and in situ observations. *J. Climate*, **18**, 3470–3482, https://doi.org/10.1175/JCLI3485.1.

Valdes, P. J., and B. J. Hoskins, 1989: Linear stationary wave simulations of the time-mean climatological flow. *J. Atmos. Sci.*, **46**, 2509–2527, https://doi.org/10.1175/1520-0469(1989)046<2509:LSWSOT>2.0.CO;2.

Vannière, B., A. Czaja, and H. F. Dacre, 2017b: Contribution of the cold sector of extratropical cyclones to mean state features over the Gulf Stream in winter. *Quart. J. Roy. Meteor. Soc.*, **143**, 1990–2000, https://doi.org/10.1002/qj.3058.

Vannière, B., A. Czaja, H. Dacre, and T. Woollings, 2017a: A "Cold Path" for the Gulf Stream-Troposphere connection. *J. Climate*, **30**, 1363–1379, https://doi.org/10.1175/JCLI-D-15-0749.1.

Wagawa, T., S. I. Ito, Y. Shimizu, S. Kakehi, and D. Ambe, 2014: Currents associated with the quasi-stationary jet separated from the Kuroshio Extension. *J. Phys. Oceanogr.*, **44**, 1636–1653, https://doi.org/10.1175/JPO-D-12-0192.1.

Wallace, J. M., and Q. Jiang, 1987: On the observed structure of the interannual variability of the atmosphere/ocean climate system. Atmospheric and Oceanic Variability, H. Cattle, Ed., Royal Meteorological Society, 17–43.

Wallace, J. M., T. P. Mitchell, and C. Deser, 1989: The influence of sea-surface temperature on surface wind in the eastern equatorial Pacific: Seasonal and interannual variability. *J. Climate*, **2**, 1492–1499, https://doi.org/10.1175/1520-0442(1989)002<1492:TIOSST>2.0.CO;2.

Walter, K., U. Luksch, and K. Fraedrich, 2001: A response climatology of idealized midlatitude thermal forcing experiments with and without a storm track. *J. Climate*, **14**, 467–484, https://doi.org/10.1175/1520-0442(2001)014<0467:ARCOIM>2.0.CO;2.

Wang, J. B., L. Fan, and Q. Y. Liu, 2010: Relationship between North Pacific SST anomalies and the atmospheric circulation anomalies in January 2008. *Journal of Ocean University of China*, **9**, 11–15, https://doi.org/10.1007/s11802-010-0011-2.

Wang, Y. X., X. Y. Yang, and J. Y. Hu, 2016: Position variability of the Kuroshio Extension sea surface temperature front. *Acta Oceanologica Sinica*, **35**, 30–35, https://doi.org/10.1007/s13131-016-0909-7.

Wen, N., Z. Y. Liu, Q. Y. Liu, and C. Frankignoul, 2010: Observed atmospheric responses to global SST variability modes: A unified assessment using GEFA. *J. Climate*, **23**, 1739–1759, https://doi.org/10.1175/2009JCLI3027.1.

Williams, R. G., C. Wilson, and C. W. Hughes, 2007: Ocean and atmosphere storm tracks: The role of eddy vorticity forcing. *J. Phys. Oceanogr.*, **37**, 2267–2289, https://doi.org/10.1175/JPO3120.1.

Willison, J., W. A. Robinson, and G. M. Lackmann, 2015: North Atlantic storm-track sensitivity to warming increases with model resolution. *J. Climate*, **28**, 4513–4524, https://doi.org/10.1175/JCLI-D-14-00715.1.

Wills, S. M., and D. W. J. Thompson, 2018: On the observed relationships between wintertime variability in Kuroshio-Oyashio Extension sea surface temperatures and the atmospheric circulation over the North Pacific. *J. Climate*, **31**, 4669–4681, https://doi.org/10.1175/JCLI-D-17-0343.1.

Wilson, C., B. Sinha, and R. G. Williams, 2009: The effect of ocean dynamics and orography on atmospheric storm tracks. *J. Climate*, **22**, 3689–3702, https://doi.org/10.1175/2009JCLI2651.1.

Woollings, T., B. Hoskins, M. Blackburn, D. Hassell, and K. Hodges, 2010: Storm track sensitivity to sea surface temperature resolution in a regional atmosphere model. *Climate Dyn.*, **35**, 341–353, https://doi.org/10.1007/s00382-009-0554-3.

Wu, Y. T., M. Ting, R. Seager, H. P. Huang, and M. A. Cane, 2011: Changes in storm tracks and energy transports in a warmer climate simulated by the GFDL CM2.1 model. *Climate Dyn.*, **37**, 53–72, https://doi.org/10.1007/s00382-010-0776-4.

Xie, S. P., 2004: Satellite observations of cool ocean-atmosphere

interaction. *Bull. Amer. Meteor. Soc.*, **85**, 195–208, https://doi.org/10.1175/BAMS-85-2-195.

Xie, S. P., T. Kunitani, A. Kubokawa, M. Nonaka, and S. Hosoda, 2000: Interdecadal thermocline variability in the North Pacific for 1958–97: A GCM simulation. *J. Phys. Oceanogr.*, **30**, 2798–2813, https://doi.org/10.1175/1520-0485(2000)030<2798:ITVITN>2.0.CO;2.

Xu, H. M., M. M. Xu, S. P. Xie, and Y. Q. Wang, 2011: Deep atmospheric response to the spring Kuroshio over the East China Sea. *J. Climate*, **24**, 4959–4972, https://doi.org/10.1175/JCLI-D-10-05034.1.

Yao, Y., Z. Zhong, and X. Q. Yang, 2016: Numerical experiments of the storm track sensitivity to oceanic frontal strength within the Kuroshio/Oyashio Extensions. *J. Geophys. Res.: Atmos.*, **121**, 2888–2900, https://doi.org/10.1002/2015JD024381.

Yao, Y., Z. Zhong, and X. Q. Yang, 2018: Impacts of the subarctic frontal zone on the North Pacific storm track in the cold season: An observational study. *International Journal of Climatology*, **38**, 2554–2564, https://doi.org/10.1002/joc.5429.

Yao, Y., Z. Zhong, X. Q. Yang, and X. G. Huang, 2019: Seasonal variations of the relationship between the North Pacific storm track and the meridional shifts of the subarctic frontal zone. *Theor. Appl. Climatol.*, **136**, 1249–1257, https://doi.org/10.1007/s00704-018-2559-5.

Yasuda, I., 2003: Hydrographic structure and variability in the Kuroshio-Oyashio transition area. *Journal of Oceanography*, **59**, 389–402, https://doi.org/10.1023/A:1025580313836.

Yin, J. H., 2005: A consistent poleward shift of the storm tracks in simulations of 21st century climate. *Geophys. Res. Lett.*, **32**, L18701, https://doi.org/10.1029/2005GL023684.

Yuan, L., and Z. N. Xiao, 2018: Impact of the Kuroshio Extension oceanic front on autumn and winter surface air temperatures over North America. *Journal of Ocean University of China*, **17**, 713–720, https://doi.org/10.1007/s11802-018-3468-z.

Yuan, X. J., and L. D. Talley, 1996: The subarctic frontal zone in the North Pacific: Characteristics of frontal structure from climatological data and synoptic surveys. *J. Geophys. Res.: Oceans*, **101**, 16 491–16 508, https://doi.org/10.1029/96JC01249.

Zhai, X. M., and R. J. Greatbatch, 2006: Surface eddy diffusivity for heat in a model of the northwest Atlantic Ocean. *Geophys. Res. Lett.*, **33**, L24611, https://doi.org/10.1029/2006GL028712.

Zhang, C., H. L. Liu, C. Y. Li, and P. F. Lin, 2019a: Impacts of mesoscale sea surface temperature anomalies on the meridional shift of North Pacific storm track. *International Journal of Climatology*, **39**, 5124–5139, https://doi.org/10.1002/joc.6130.

Zhang, C., H. L. Liu, J. B. Xie, C. Y. Li, and P. F. Lin, 2020a: Impacts of increased SST resolution on the North Pacific storm track in ERA-Interim. *Adv. Atmos. Sci.*, **37**, 1256–1266, https://doi.org/10.1007/s00376-020-0072-0.

Zhang, C. H., H. L. Li, S. T. Liu, L. J. Shao, Z. Zhao, and H. W. Liu, 2015: Automatic detection of oceanic eddies in reanalyzed SST images and its application in the East China Sea. *Science China Earth Sciences*, **58**, 2249–2259, https://doi.org/10.1007/s11430-015-5101-y.

Zhang, C., H. L. Liu, J. B. Xie, P. F. Lin, C. Y. Li, Q. Yang, and J. Song, 2020b: North Pacific storm track response to the mesoscale SST in a global high-resolution atmospheric model. *Climate Dyn.*, **55**, 1597–1611, https://doi.org/10.1007/s00382-020-05343-x.

Zhang, J., and D. H. Luo, 2017: Impact of Kuroshio Extension dipole mode variability on the North Pacific storm track. *Atmos. Ocean. Sci. Lett.*, **10**, 389–396, https://doi.org/10.1080/16742834.2017.1351864.

Zhang, X., M. Mu, Q. Wang, and S. Pierini, 2017: Optimal precursors triggering the Kuroshio Extension state transition obtained by the conditional nonlinear optimal perturbation approach. *Adv. Atmos. Sci.*, **34**, 685–699, https://doi.org/10.1007/s00376-017-6263-7.

Zhang, X. Z., X. H. Ma, and L. X. Wu, 2019b: Effect of mesoscale oceanic eddies on extratropical cyclogenesis: A tracking approach. *J. Geophys. Res.: Atmos.*, **124**, 6411–6422, https://doi.org/10.1029/2019JD030595.

Zhou, G. D., 2019: Atmospheric response to sea surface temperature anomalies in the mid-latitude oceans: A brief review. *Atmos.-Ocean*, **57**, 319–328, https://doi.org/10.1080/07055900.2019.1702499.

Zhou, G. D., M. Latif, R. J. Greatbatch, and W. Park, 2015: Atmospheric response to the North Pacific enabled by daily sea surface temperature variability. *Geophys. Res. Lett.*, **42**, 7732–7739, https://doi.org/10.1002/2015GL065356.

Zhou, G. D., M. Latif, R. J. Greatbatch, and W. Park, 2017: State dependence of atmospheric response to extratropical North Pacific SST anomalies. *J. Climate*, **30**, 509–525, https://doi.org/10.1175/JCLI-D-15-0672.1.